Dissertations
Department of Chemistry
University of Eastern Finland

No. 142 (2017)

Muhammad Safdar

Manganese Oxide Based Catalytic Micromotors: Synthesis, Characterization and Applications

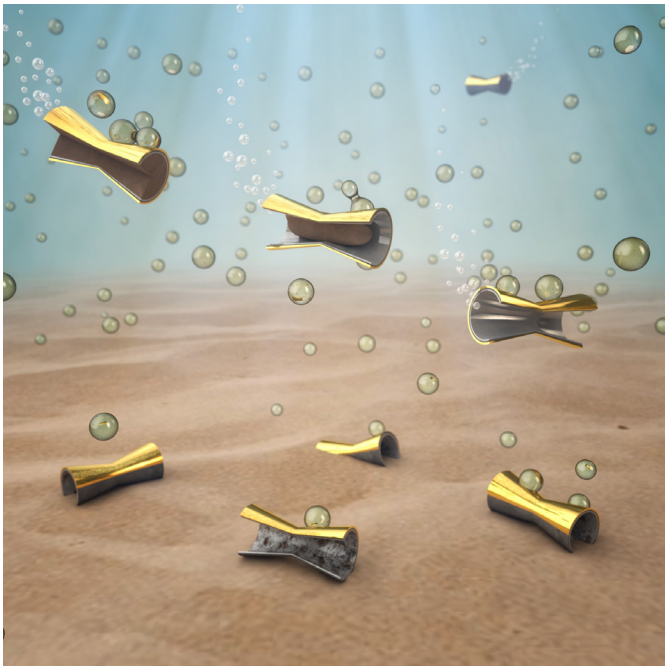

Manganese Oxide Based Catalytic Micromotors: Synthesis, Characterization and Applications

Muhammad Safdar

Department of Chemistry
University of Eastern Finland
Finland

Joensuu 2017

Muhammad Safdar
Department of Chemistry, University of Eastern Finland
P.O. Box 111, FI-80101 Joensuu, Finland

Supervisor
Prof. Janne Jänis, University of Eastern Finland

Referees
Prof. Jaakko Timonen, Aalto University
Prof. Hélder A. Santos, University of Helsinki

Opponent
Dr. Salvador Pané i Vidal, Swiss Federal Institute of Technology (ETH), Zurich

To be presented with the permission of the Faculty of Science and Forestry of the University of Eastern Finland for public criticism in Auditorium F100, Yliopistokatu 7, Joensuu, on November 16th, 2017 at 12 o'clock noon.

Copyright © 2017 Muhammad Safdar

ISBN 978-952-61-2624-1
ISSN 2242-1033

Grano Oy
Jyväskylä, 2017

ABSTRACT

Synthetic micro- and nanomotors (MNMs) are tiny devices with dimensions less than the diameter of a human hair. MNMs can undergo autonomous motion in liquid environments, which can be driven by various means such as a chemical fuel, ultrasound, light energy or magnetic field. The fuel-driven MNMs are often catalytic in nature, which cause transformation of a chemical fuel into reaction products (neutral or ionic) that lead to a self-propulsion of the particles through various mechanisms. MNMs may find use, *e.g.*, in targeted cargo transport of other molecules (*e.g.*, drug delivery), specific catalysis or chemical sensing, although their large-scale use is not yet demonstrated.

Platinum (Pt) is by far the most widely explored catalytic material for the preparation of MNMs. It decomposes hydrogen peroxide (H_2O_2) fuel into oxygen gas (O_2) and water molecules. However, Pt is an extremely rare element and suffers from some limitations, such as drastically reduced catalytic efficiency in salt-rich environments and complete inactivation of the catalytic surface due to the chemisorption of certain compounds, like thiols. This necessitates the discovery of alternate materials with similar or even better performance. Manganese oxide (MnO_2) is a catalytic material that can decompose H_2O_2 similar to Pt. Also, MnO_2 is cheap and available in large quantities. Thus, MnO_2 holds a considerable potential for the preparation of MNMs, but has been scarcely explored to date.

In this study, a variety of MnO_2-based micromotors in different morphological designs and crystalline forms were synthesized and characterized in terms of their motion behavior in solution. To demonstrate their potential for practical applications, the MnO_2 micromotors were used for the removal of organic dyes from the polluted water. The dye removal process was based on a unique effect that combined catalytic degradation (CD) and adsorptive bubble separation (ABS) processes. A dye removal efficiency of over 90% was recorded in just 1 h of operation without external mixing. Finally, MnO_2 was used as a material for protecting the conventional Pt-based micromotors from thiol toxicity. Thus, MnO_2 holds a great promise for the preparation of novel synthetic MNMs for a wide range of applications.

LIST OF ORIGINAL PUBLICATIONS

This dissertation is a summary of the following original publications I–IV.

I. Safdar, M.; Wani, O.M.; Jänis J. Manganese Oxide-Based Chemically Powered Micromotors, *ACS Appl. Mater. Interfaces* **2015**, *7*, 25580−25585.

II. Safdar, M.; Do Minh, T.; Kinnunen, N.; Jänis, J. Manganese Oxide Based Catalytic Micromotors: Effect of Polymorphism on Motion, *ACS Appl. Mater. Interfaces* **2016**, *8*, 32624−32629.

III. Wani, O.M.; Safdar, M.; Kinnunen N.; Jänis J. Dual Effect of Manganese Oxide Micromotors: Catalytic Degradation and Adsorptive Bubble Separation of Organic Pollutants, *Chem. Eur. J.* **2016**, *22*, 1244–1247.

IV. Do Minh, T.; Safdar, M.; Jänis, J. Protection of Platinum-Based Micromotors from Thiol Toxicity by Using Manganese Oxide, *Chem. Eur. J.* **2017**, *23*, 8134–8136.

The author's contribution to the publications:

The research presented in the original publications I–IV is an outcome of the author's own ideation and discussions between the author, supervisor and coauthors. The author had a leading role in designing and performing the experimental work. The syntheses, motion tracking, particle trajectory analysis and interpretation of the results were conducted by the author in collaboration with the coauthors. The characterization of materials was mainly performed by the author, except the X-ray diffraction (II and III) and mass spectrometric analyses (III). The publications were written by the author in collaboration with the supervisor.

CONTENTS

ABSTRACT **3**
LIST OF ORIGINAL PUBLICATIONS **4**
ABBREVIATIONS **6**
1. INTRODUCTION **7**
1.1. BACKGROUND 7
1.2. CHALLENGES OF MOTION AT THE MICROSCALE 8
1.3. TYPES OF MICRO- AND NANOMOTORS 8
1.3.1. FUEL-FREE MNMs 8
1.3.2. FUEL-DRIVEN MNMs 9
1.4. MATERIALS FOR SYNTHESIS OF MNMs 11
1.4.1. METALS 11
1.4.2. METAL OXIDES 12
1.4.3. ENZYMES 13
1.5. FABRICATION OF MNMs 13
1.5.1. PHYSICAL VAPOR DEPOSITION 13
1.5.2. ELECTROCHEMICAL DEPOSITION 14
1.5.3. COLLOIDAL SYNTHESIS 14
1.6. APPLICATIONS OF MNMs 14
1.6.1. BIOMEDICAL APPLICATIONS 14
1.6.2. ENVIRONMENTAL APPLICATIONS 15
2. AIMS OF THE STUDY **16**
3. EXPERIMENTAL **17**
3.1. MATERIALS 17
3.2. EQUIPMENT 17
3.3. SYNTHESIS [I, II] 17
3.4. REMOVAL OF ORGANIC DYES FROM POLLUTED WATER [III] 19
3.5. PROTECTION OF PLATINUM BASED MICROMOTORS FROM THIOL TOXICITY [IV] 19
4. RESULTS AND DISCUSSION **20**
4.1. SYNTHESIS AND CHARACTERIZATION OF NOVEL MANGANESE OXIDE BASED MICROMOTORS [I, II] 20
4.2. REMOVAL OF ORGANIC DYES FROM POLLUTED WATER [III] 25
4.3. PROTECTION OF PLATINUM BASED MICROMOTORS FROM THIOL TOXICITY [IV] 28
5. CONCLUSIONS **31**
ACKNOWLEDGEMENTS **33**
REFERENCES **34**

ABBREVIATIONS

MNMs	Micro- and nanomotors
SDS	Sodium dodecyl sulfate
SiO_2	Silicon dioxide
H_2O_2	Hydrogen peroxide
PEDOT	3,4-ethylenedioxythiophene
R6G	Rhodamine 6G
MB	Methylene blue
µm	Micrometer
nm	Nanometer
GOx	Graphene oxide
CD	Catalytic degradation
ABS	Adsorptive bubble separation
PVD	Physical vapor deposition
SEM	Scanning electron microscopy
EDX	Energy dispersive X-ray spectroscopy
XRD	X-ray diffraction
WE	Working electrode
RE	Reference electrode
CE	Counter electrode
PC	Polycarbonate
NPs	Nanoparticles
bdl s^{-1}	Body lengths per second

1. INTRODUCTION

1.1. BACKGROUND

The science fiction movie "Fantastic Voyage" in 1966 introduced a visionary concept of miniaturizing devices down to the micrometer scale for accomplishing incredible tasks (Figure 1).[1,2] The plot of the movie was based on the miniaturization of a submarine crew comprised of a team of surgeons, who were shrunk to the micrometer size and subsequently injected into the blood stream of an injured scientist to treat a damage in his brain. The movie eventually won two Academy Awards in 1966.

Figure 1. Poster of the movie "Fantastic Voyage" in 1966 (reprinted with permission).[1]

Nature has created its own biological machinery, known as motor proteins, to perform specific physiological functions such as muscle contraction and intracellular transport of organelles or vesicles. Few typical examples of such proteins are kinesins, dyenins and myosin. The transport of motor proteins takes places through dedicated tracks, called cytoskeletal microtubules.[3] The dimensions of motor proteins are typically in the nanometer range. Moreover, larger natural microswimmers, such as bacteria or sperm cells, utilize motor proteins to drive flagella or cilia for their free and fast motility. For instance, a bacterium *Escherichia coli* with a size of a few microns can move at a speed of ~22 $\mu m\ s^{-1}$.[4]

The miniaturization of macroscopic objects is no more a fantasy of the science fiction movie of 1966. About four decades later, the world has witnessed a rapid emergence of tiny synthetic devices that can autonomously move in liquid environments while accomplishing different tasks. During the past decade, there has been a tremendous interest to design and further synthesize self-propelling micro- and nanoscale particles, known as micro- and nanomotors (MNMs), having a wide variety of applications in chemistry, medicine and environmental sciences.[5–11]

1.2. CHALLENGES OF MOTION AT THE MICROSCALE

At the macroscale, the objects make use of inertial forces to move through fluids. This means that the momentum imparted to the body continues to operate for some time. Hence, intermittent work is needed to sustain the motion. The body tends to continue its motion because the inertia is strong enough to counter the viscosity of the fluid. However, this scenario does not hold true at the microscale due to the absence of the inertial forces.[12] Thus, viscous forces become dominant. Under such conditions, the motion by a conventional reciprocating mechanism (*i.e.*, back and forth movement) would produce zero net displacement.[13] This implies that the movement at the microscale has to be performed in a nonreciprocating manner.

The thermally driven random motion of solvent molecules also poses a challenge to the motion of micro- and nanoscale particles. The Brownian motion interferes with the directional motion of MNMs as the temperature increases or the particle size decreases. As a result, the object adopts a random motion trajectory due to a frequent geometrical reorientation. This necessitates the need for external means to control the orientation and directionality of MNMs for applications that may require propulsion towards a particular target site.

1.3. TYPES OF MICRO- AND NANOMOTORS

Synthetic MNMs that require an external means of actuation are known as fuel-free MNMs. In contrast, MNMs that need a chemical substance to self-generate an asymmetric force are called fuel-driven MNMs.

1.3.1. FUEL-FREE MNMs

External energy sources such as magnetic fields, ultrasound or light irradiation can be used to power up MNMs based on the choice of materials used for their fabrication and their geometrical designs.

Magnetically driven MNMs

Low magnetic fields are noninvasive and routinely used in biomedical diagnostics. The liquid medium and the body fluids do not absorb magnetic fields. Thus, actuation of the MNMs can be performed in both *in vitro* and *in vivo* applications.[14–16] The motion of magnetic MNMs relies upon their specific body shape (*e.g*. helical, twist or screw), as exemplified in Figure 2A. Under the influence of a rotating magnetic field that applies a continuous torque to the particle, a rotational motion along their longitudinal axis translates to a net displacement due to the resulting “screw-type” motion. The fabrication of magnetic MNMs is typically performed by thin film deposition or electrochemical deposition methods.[17–19] A strong permanent magnet or an assembly of electromagnetic coils creates an external magnetic field to drive the motion. In the case of a permanent magnet, the strength of the applied magnetic field is variable by changing the distance between the magnet and the particle. In contrast, the field strength by using

electromagnetic coils is tunable by modulating the amplitude of the current flowing through a fixed assembly of coils.

Light-driven MNMs

Light is a renewable form of energy that can provide power to the synthetic MNMs by various mechanisms.[20] The momentum transfer of the impinging photons can lead to rotational and translational motion of the microstructures.[21,22] Light can generate an interfacial tension gradient across the particle surface modified with a photosensitive material, which leads to a net directional motion towards a region of lower interfacial tension.[23] Light-induced photothermal effect, also known as self-thermophoresis, is another unique effect that leads to the propulsion of MNMs by creating a temperature gradient across the particle surface (Figure 2B).[24,25] Photocatalytic materials, such as titanium dioxide and silver/silver chloride, can generate a gradient of electrolytes across the particles under the UV light irradiation, resulting in propulsion.[26–28] In addition, polymeric soft MNMs can undergo motion due to light-induced deformations within the molecular networks of the photosensitive materials.[29,30]

Ultrasonically driven MNMs

Ultrasound is another noninvasive source of energy which is common in biomedical diagnostics. Sound waves in the MHz frequency range are safe and powerful, and can be used for the manipulation of a matter at the microscale.[31] A piezoelectric transducer converts electrical signals into mechanical vibrations of the ceramic element that generates ultrasound waves.[32] Ultrasound is applicable either as a surface acoustic wave or bulk acoustic wave by using distinct transducer arrangements. The application of an ultrasound standing wave generates zones of high and low acoustic pressure within the sample container. The low-pressure zones are called the nodal points and the plane in which the nodal points are arranged is called the nodal or the levitation plane (Figure 2C). The MNMs essentially require a geometrical asymmetry to experience a net acoustic pressure force required for motion.[33–35] An asymmetric rod-like geometry can experience a net acoustic force that leads to the motion. On the other hand, a symmetric spherical geometry cannot experience a pressure difference, and thus cannot undergo acoustic propulsion.

1.3.2. FUEL-DRIVEN MNMs

Fuel-driven MNMs are composed of a catalytic material that triggers a chemical reaction upon interaction with another chemical substance (*i.e.*, a fuel) present in the liquid environment. Hydrogen peroxide (H_2O_2) is a typical example of a chemical fuel used to drive MNMs. The motion can be caused by a few distinct mechanisms.

Self-diffusiophoresis

A propulsion mechanism that proceeds through a concentration gradient of the reaction products produced by an asymmetric nanoparticle is called self-diffusiophoresis. If the

products are neutral or charged, the mechanism is more specifically referred to as neutral or ionic self-diffusiophoresis, respectively.[36] In neutral self-diffusiophoresis, catalytic hemisphere of a Janus particle (*i.e.*, a spherical micro- or nanoparticle with chemically or physically two distinct faces) converts a fuel into products and undergoes a generalized repulsive interaction over a certain length scale. This causes a phoretic flow of the surrounding liquid from the inert side of the particle towards the catalytic side and establishes a flux of the product molecules towards the regions of lower product concentration. The asymmetry in the product distribution is accompanied by an asymmetry of the repulsive interactions acting around the particle, which exerts a propelling force.[37,38] An example of the neutral self-diffusiophoresis is the oxidation of H_2O_2 into H_2O and O_2 by the platinum/silica (Pt/SiO_2) Janus microspheres depicted in Figure 2D.[39]

The ionic self-diffusiophoresis is based on the electric and pressure gradients arising from the differential diffusion of specific cations and anions produced by the MNM. The ionic diffusiophoresis is exhibited by Ag/SiO_2 particles that produce an ionic gradient in a given direction upon UV light irradiation.[26,40,41]

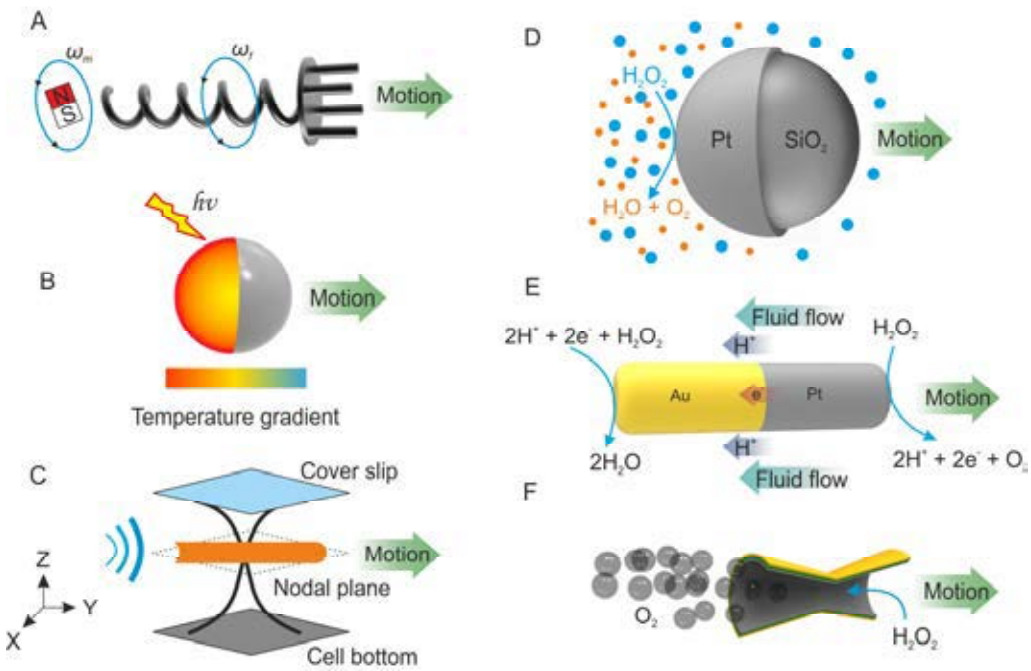

Figure 2. (A-C) Schematic illustration of fuel free MNMs driven by magnetic, light-induced thermophoresis and ultrasonic actuation mechanisms, respectively. (D-F) Fuel driven MNMs propelled by self-diffusiophoresis, self-electrophoresis and bubble formation mechanisms, respectively.

Self-electrophoresis

A propulsion mechanism that relies on a locally created electric field and a charged particle surface is known as self-electrophoresis. Self-electrophoresis is typically exhibited by bimetallic MNMs, which oxidize H_2O_2 at the anodic segment (*e.g.*, platinum) while reduce it at the cathodic segment (*e.g.*, gold).[42,43] As a result, the anode produces a higher concentration of protons, rendering the cathode proton deficient. This establishes an asymmetric charge distribution that points towards the Au segment. As the protons migrate towards the cathode, they drag the fluid along with them, which results in a motion of the MNM in the opposite direction (Figure 2E). Such particles move with the Pt segment facing forward.

Bubble-induced propulsion

In a favorable geometry, *e.g.* a microtube or a microparticle with sufficuent size, the gaseous products (*e.g.* O_2) of a chemical reaction may undergo nucleation, bubble formation/growth and a subsequent expulsion to provide a strong thrust to the particle for motion,[44–46] as depicted in Figure 2F. The presence of a small quantity of a surfactant is often crucial to facilitate bubble formation.[47] The bubble-propelled micromotors exhibit faster motion compared to those driven by self-electrophoresis or self-diffusiophoresis mechanisms.

1.4. MATERIALS FOR SYNTHESIS OF MNMs

1.4.1. METALS

Pt is by far the most extensively used catalytic material for the fabrication of MNMs. The pioneering work of Whitesides *et al.* introduced bubble-propelled hemicylindrical plates, composed of a patterned polydimethoxysilane and a Pt surface, placed at the air–liquid interface.[48] This development was followed by Pt/Au segmented nanorods that were propelled by self-electrophoresis.[42] The speed of the nanorods can be remarkably improved by incorporating carbon nanotubes into the Pt segment of the nanorods.[49] Janus Pt/SiO_2 MNMs propel by self-generated diffusiophoresis.[50] A rough catalytic surface can cause an accelerated motion of the spherical Janus MNMs.[39,51] Tubular geometries with an inner Pt surface undergo very fast motion due to the bubble-propulsion mechanism.[44] Their speeds are further enhanced at a physiological temperature due to a consequent increase in the reaction rate and a decrease in the viscosity of the medium.[52] Pt-based nanoparticles are also used to prepare MNMs.[53–55] Although fuel-driven MNMs based on Pt have high catalytic activity, they suffer from some serious limitations. First, Pt is an extremely rare element, making it one of the most expensive materials on Earth. The practical environmental applications of MNMs often require large quantities, which limits the use of expensive materials. In addition, the efficiency of Pt based MNMs is greatly reduced in salt rich environments. Another serious drawback of the Pt-based micromotors is their tendency towards thiol-containing compounds that chemisorb and block the catalytic sites.[56]

Silver (Ag) can catalyze H_2O_2 decomposition in a manner similar to Pt and produces a recoil of bubbles that cause motion of MNMs. Micromotors based on a single crystal polycaprolactone architecture, decorated with silver nanoparticles (AgNPs), moved at a speed of 80 μm s^{-1} in 15% H_2O_2.[57] Commercially obtained anisotropic Ag microparticles also exhibited a similar bubble-propelled motion.[58] Microtubular structures composed of a Ag segment moved with an average speed of 252 μm s^{-1} (*i.e.*, 20 body lengths s^{-1}) in 3% fuel. Despite a low cost, Ag-based MNMs can potentially contribute to aquatic toxicity which poses problems for their use in environmental applications.

Zinc (Zn) reacts with acids to produce Zn^{2+} ions and evolves hydrogen (H_2) gas that can propel MNMs by bubble formation.[59,60] Metallic magnesium (Mg) is stable in ambient atmosphere due to rapid formation of an outer $Mg(OH)_2$ passivation layer. However, immersion of Mg particles in a bicarbonate (HCO_3^-) environment results in dissolution of the passivation layer. The bare Mg surface can reduce water molecules to produce H_2 gas bubbles.[61] A similar effect is observed in the presence of Cl^- ions that cause a pitting corrosion of the passivation layer.[62] Both Mg and Zn are promising materials for the design of MNMs propelled by consuming biocompatible chemical fuels. However, due to the fast self-degradation of these materials, Mg and Zn based MNMs exhibit a lifetime of up to a few minutes only. Also, these MNMs need to be stored in organic solvents to avoid undesired reactions.

Aluminum (Al) is another material that can reduce water similar to Mg. The oxide passivation layer around Al particles can be removed by forming an Al-Ga alloy on the particle surface using microcontact printing of Ga metal. When placed in water, the Al-Ga alloy system can reduce water to form H_2 bubbles required for propulsion.[63]

1.4.2. METAL OXIDES

The use of metal oxides for preparation of MNMs is less common due to a very limited number of materials with desired catalytic properties. Manganese oxide (MnO_2) is a low-cost and very abundant material that is catalytic in nature and can decompose H_2O_2. The earliest report on MnO_2-based bubble-propelled micromotors introduced the use of commercially available MnO_2 particles.[58] These particles required at least 12% of fuel to reach a speed of ~50 μm s^{-1}. Micromotors based on MnO_2/graphene composite achieved a speed of ~48 μm s^{-1} in 2.5% fuel and 0.33% surfactant, which represents an improved fuel efficiency as compared to the MnO_2 particles from the previous study.[64,65] Pot-like $MnFe_2O_4$ hollow particles with an inner catalytic surface could move with a speed of 260 μm s^{-1} in 2% fuel and 0.1% surfactant.[66] The bubbles formed inside of the hollow particle were eject through the holes in the particle surface. Paper-based tubular micromotors decorated with MnO_2 nanoparticles could also move in H_2O_2 solution.[67] Their maximum speed was only up to 5.5 body lengths (bdl) s^{-1} in 16% fuel solution, and a lifetime of ~6 min. However, the existing MnO_2 based MNMs are less efficient and require higher concentrations of fuel to undergo efficient motion. In addition, the potential of MnO_2 based MNMs for practical applications also needs to be explored.

1.4.3. ENZYMES

Enzymes are biocatalysts that operate in a fashion similar to inorganic catalysts. Catalase is a biological equivalent to Pt that oxidizes H_2O_2 and efficiently propels MNMs.[68,69] Glucose oxidase converts glucose into gluconic acid and H_2O_2 and drives MNMs as well.[70] Urease, which converts urea into ammonia and carbon dioxide, is another potential candidate to drive MNMs of various geometries.[71,72] Enzymes can be a very good alternate to metals and metal oxides for MNM preparation for certain applications. However, a rapid inactivation of enzymes in harsh environmental conditions may seriously limit the operational life time of enzyme-based MNMs.

1.5. FABRICATION OF MNMs

1.5.1. PHYSICAL VAPOR DEPOSITION

Physical vapor deposition (PVD) methods allow deposition of thin films of materials on surfaces. The materials are vaporized by supplying a high-temperature or a plasma. The vapors reach the substrate surface in vacuum and undergo a condensation to form a thin film. The most common PVD techniques used for the fabrication of MNMs are sputtering and electron beam evaporation (Figure 3). Sputtering relies on the bombardment of a material source (target) with an ionized inert gas, such as argon (Ar). The transfer of kinetic energy of the ionized gas ejects atoms from the target material, which then forms a thin layer on a substrate surface. In the case of electron beam evaporation, a beam of electrons is continuously focused onto a crucible containing the target material to be deposited. The electron beam heats the target to form vapors of atoms which then condense at the substrate surface to be coated. PVD methods are extensively used for the preparation of rolled-up tubular and Janus MNMs.[44,73–77] PVD methods can deposit various materials such as metals (*e.g.*, Pt, Au, Ni, Ti and Cr), metal nitrides and organic materials.

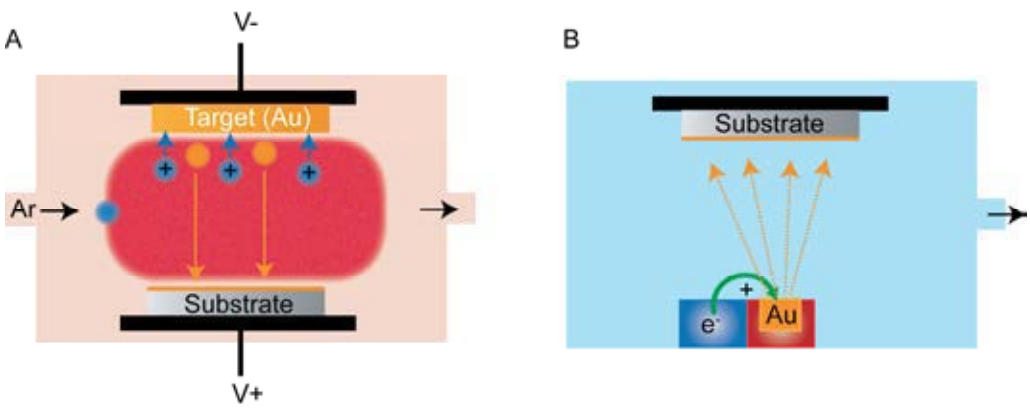

Figure 3. Schematic of the principles of typical PVD methods used for MNMs preparation. (A) Sputtering relies on the creation of argon plasma. The ionized argon gas hits the metal target and

dislodge atoms that deposit on the substrate surface to form a thin film. (B) Electron beam evaporation of metal by heating the target material using a focused beam of electrons.

1.5.2. ELECTROCHEMICAL DEPOSITION

Electrochemical deposition can be used to prepare not only thin films but also three-dimensional micro- and nanostructures. For fabrication of MNMs, electrodeposition of desired materials typically needs to be performed inside a template. This method is referred to as template-assisted electrodeposition. The most widely used templates for electrodeposition of MNMs are porous polycarbonate (PC) or anodized aluminum oxide filtration membranes.[46,78] Because these templates are nonconductive, a metal film is deposited by sputtering onto one of the sides of the template, which serves as a working electrode (WE). The template is assembled in a plating cell and soaked in an electrolyte solution that contains ions of the material to be deposited. By supplying current to the WE, the metal ions are reduced into their elemental form which get deposited onto the pore surfaces of the membrane. Other materials that can be deposited by the electrochemical deposition method include conducting polymers and graphene oxide (GOx). Electrochemical preparation of catalytic tubular structures is often done by first depositing a layer of GOx or a conducting polymer. This can be followed by depositing a Ni layer to incorporate a magnetic functionality for a control over the direction of motion. Finally, an active/catalytic material is deposited. After removing the thin metal film WE by hand polishing, the template can be dissolved to release the MNMs. In terms of the particle geometry, this method can produce tubular, nanowire- or rod-like MNMs.[60,79,80] The dimensions of MNMs can be tailored by selecting a template of a desired pore size.

1.5.3. COLLOIDAL SYNTHESIS

Colloidal synthesis methods for MNMs include layer-by-layer (LBL) assembly, encapsulation of nanoparticles (NPs) and chemical co-precipitation.[81,82] In the LBL assembly, the materials with opposite charges assemble in the form of alternating layers. The assembly takes place on a template particle to produce a defined geometry, such as a microcapsule.[83,84] This can be followed by the immobilization of catalyst NPs or an enzyme to drive the motion. The asymmetric encapsulation of the catalyst NPs onto or inside another particle is another simple approach to prepare MNMs.[57,85] The chemical co-precipitation method for preparation of MNMs is rarely used.

1.6. APPLICATIONS OF MNMs

1.6.1. BIOMEDICAL APPLICATIONS

Conventional drug delivery systems rely on passive transport and systemic circulation mechanism that lacks the force required for tissue penetration and targeted release of the therapeutic substance.[86] MNMs possess attractive features to meet the requirements for the targeted payload delivery due to their active propulsion, navigation and drug release capabilities. MNMs can self-propel and release the loaded therapeutic agents

only to the unhealthy cells.[55,87–89] *In vivo* applications of drug loaded MNMs to treat stomach infection also exist.[90–92] The advantage of Zn- and Mg-based MNMs is their instant propulsion in body fluids without an external chemical fuel, their transient nature and, moreover, formation of non-toxic byproducts. Enzyme-based MNMs that also can utilize biological fuels, such as glucose or urea, are very potential candidates for active biomedical drug delivery.[70,71] Besides the drug delivery applications, MNMs offer various other possibilities, such as their use in manipulation of cells,[93] isolation of bacteria,[94] capture and transport of proteins,[95] immunoassays,[96–99] or minimally invasive surgery.[100]

1.6.2. ENVIRONMENTAL APPLICATIONS

Synthetic MNMs have demonstrated a great potential for environmental remediation applications due to their ability to locally induce mixing for an enhanced mass transfer. This feature greatly benefits water remediation processes that are mostly diffusion limited and need external means of mixing. Alkanethiol-functionalized Au/Pt-based microtubular motors can navigate, capture and transport oil microdroplets for cleaning of oil spills.[56] However, due to the chemisorption of thiol-containing compounds, the Pt surface becomes rapidly poisoned and the efficiency of MNMs reduces drastically. Bilayered Fe/Pt-microtubes perform Fenton-like degradation of organic dyes, such as Rhodamine 6G (R6G).[101] The intermixing caused by the motion of micromotors leads to the accelerated degradation of the pollutant as compared to the diffusion limited process. The effectiveness of MNMs to sense and detoxify nerve agents and other toxic substances has also proven a great potential.[102,103] In addition, dynamic removal of heavy metal contaminants from waste waters is another exciting application of the MNMs.[104,105] Furthermore, the antibacterial effect of MNMs can also be used for killing pathogenic bacteria present in the ecosystem.[9,106,107]

2. AIMS OF THE STUDY

The aim of this study was to explore MnO_2 as a material for the synthesis of new types of micromotors and their potential applications, especially in environmental remediation. Manganese oxide exists in a large number of different crystalline forms (polymorphs) which may have different catalytic properties. Thus, an evaluation of the motion behavior of MnO_2 micromotors composed of distinct polymorphic forms was made. Furthermore, the use of MnO_2 as a protective material for platinum-based micromotors against a thiol-induced catalyst poisoning was characterized.

The specific aims of the study were as follows:

1. To prepare MnO_2-based micromotors with different geometrical designs by using a template-assisted electrochemical deposition and colloidal synthesis methods, and to study their motion behavior in response to the varying concentrations of fuel.
2. To study the effect of polymorphism on the motion of MnO_2-based micromotors in different liquid environments.
3. To demonstrate the potential of MnO_2-based micromotors for the removal of organic dyes from contaminated water.
4. To protect Pt-based tubular micromotors with MnO_2 against the chemisorption of thiol-containing compounds.

3. EXPERIMENTAL

3.1. MATERIALS

Commercial manganese dioxide (MnO_2) particles (average diameter ~10 μm), Rhodamine 6G (R6G) and Methylene blue (MB) were purchased from Alfa Aesar GmbH (Karlsruhe, Germany). Manganese(II) acetate tetrahydrate ≥99%,, 3,4-ethylenedioxythiophene (EDOT) 97%, Manganese sulphate monohydrate, ammonium bicarbonate ≥99.5%, potassium permanganate ($KMnO_4$) ≥99%, sodium dodecyl sulfate (SDS) ≥99%, potassium nitrate ≥99% and Triton™ X-100 were all purchased from Sigma-Aldrich (Missouri, USA). Sodium sulphate 99%, nickel sulfamate tetrahydrate 98%, boric acid 99.5%, graphene oxide (GOx) dispersion, and 1-octadecanethiol were also from Sigma-Aldrich. Hydrogen peroxide (30%) was purchased from Merck (Darmstadt, Germany). Porous polycarbonate (PC) membranes of an average pore diameter of 5 μm were purchased from Whatman Inc. (NY, USA). Alumina slurry was a gift by Saint-Gobain Ceramic Materials (Worcester, MA, USA). Ultrapure water (Milli-Q) was used in all experiments.

3.2. EQUIPMENT

The samples were characterized using a Hitachi S4800 field-emission scanning electron microscope (SEM) equipped with a Thermo Electron energy-dispersive X-ray spectroscopy (EDS) device. The videos for tracking the motion were recorded at 25 frames per second using an Olympus BX51 microscope (5× objective) and a Thorlabs DCC1645C CMOS camera. The videos were edited by Virtual Dub 1.10.4 software. Fiji software was used to manually track the speeds of the micromotors and to extract time-lapse images.[108] The Au coating was performed with Cressington 208HR sputtering system. An Autolab Potentiostat PGSTAT 20 was used for electrodeposition. The mass spectra were obtained with a 12-T Bruker Solarix-XR instrument (Bruker Daltonics GmbH, Bremen, Germany).

3.3. SYNTHESIS [I, II]

Electrochemical synthesis of manganese oxide microtubes and rods

Template-assisted electrodeposition of MnO_2 was carried out by first sputtering a 75 nm thick Au layer onto one side of the PC membrane to serve as a working electrode. An Ag/AgCl and a Pt wire were used as reference and counter electrodes, respectively. The PC membrane was placed on a flat strip of aluminium foil serving as the electrical contact, and was assembled into a custom made electroplating cell. MnO_2 microrods were grown potentiostatically using a potential of +0.75 V for 1 C charge, from a plating solution containing 10 mM manganese (II) acetate. For MnO_2 microtubes, an outer poly(3,4-ethylenedioxythiophene) PEDOT layer was deposited potentiostatically using a potential of +0.8 V for 0.25 C charge, from a plating solution containing 15 mM EDOT, 7.5 mM KNO_3 and 100 mM SDS. This was followed by the deposition of MnO_2 using a potential of +0.75 V for 0.3 C charge, from a plating solution containing 10 mM

manganese (II) acetate solution. Following the deposition, the gold layer was removed by gently polishing with alumina slurry. The templates were dissolved in methylene chloride for 10 minutes to release the motors. The micromotors were collected by centrifugation at 6000 rpm and were repeatedly washed with methylene chloride, ethanol and ultrapure water.

Synthesis of MnO_2@$MnCO_3$ particles

Spherical particles with a MnO_2 shell were prepared using $MnCO_3$ particles as template and are referred to as MnO_2@$MnCO_3$. Manganese sulphate monohydrate (1 mmol) and ammonium bicarbonate (10 mmol) were dissolved separately in 70 mL of MilliQ water. Ethanol (7 mL) was added to manganese sulphate solution with stirring, until it was dispersed completely, followed by addition of ammonium bicarbonate solution at room temperature. In about 3 minutes, the solution turned milky. The reaction mixture was further maintained at room temperature for 3 hours and the $MnCO_3$ microspheres were collected by centrifugation and washed repeatedly with ethanol and water. Then, the suspension of $MnCO_3$ template particles was added to 5 mL of 0.032 M $KMnO_4$ solution, shaken vigorously and incubated for 6 hours. The resulting MnO_2@$MnCO_3$ particles were collected by centrifugation, washed, and dried overnight at 60 °C.

Synthesis of hollow MnO_2 particles

The $MnCO_3$ core of the MnO_2@$MnCO_3$ particles was removed by incubation in 0.01 M hydrochloric acid, which produced hollow MnO_2 particles. The collected particles were re-oxidized by mixing with aqueous $KMnO_4$ solution, overnight. The hollow particles were separated by centrifugation, washed and dried at 60 ^{o}C.

Hydrothermal synthesis of MnO_2

Hierarchically porous MnO_2 particles were synthesized as follows.[109] In a typical synthesis, 0.625 g of $KMnO_4$ was dissolved in 56 mL of ultrapure water. To this solution, 1.4 mL of concentrated hydrochloric acid was added under vigorous mixing. The mixed solution was maintained at room temperature for 30 minutes and was transferred to a 70 mL Teflon-lined autoclave, which was then kept at 80 ^{o}C for 10 h. After cooled down to room temperature, the precipitate was washed thoroughly with ultrapure water and ethanol. The dark brown powder was obtained after drying in an oven at 60 ^{o}C overnight.

Fabrication of Mn_2O_3 particles

The $MnCO_3$ particles previously prepared by co-precipitation method were converted into Mn_2O_3 by calcination at 600 ^{o}C for 4 h at a heating rate of 10 ^{o}C/min in air atmosphere.

3.4. REMOVAL OF ORGANIC DYES FROM POLLUTED WATER [III]

Commercial MnO_2 microparticles were used as micromotors without any further modification. The remediation experiments were carried out in 50 mL beakers containing a total reaction volume of 10 mL. The reaction mixture consisted of 5 mg of MnO_2 microparticles, 2500 µL of dye stock solution (C_{MB} =125 mg L^{-1} or/and C_{R6G} = 160 mg L^{-1}), 5834 µL of H_2O and 1666 µL of 30% H_2O_2, making the final fuel concentration of 5 % (v/v). In the second experiment, 200 µL of H_2O was replaced with 200 µL of 5% (w/v) SDS to reach a final SDS concentration of 0.1% to facilitate the formation and accumulation of bubbles. For absorbance measurements, two 200-µL aliquots of the reaction mixture were taken at t = 0 and 60 min, which were diluted to 2 mL with ultrapure water prior to the analysis.

3.5. PROTECTION OF PLATINUM BASED MICROMOTORS FROM THIOL TOXICITY [IV]

The Au-sputtered PC membrane template was assembled in an electroplating cell. An aqueous solution of 0.1 mg mL^{-1} of GOx in 0.5 M sodium sulphate (Na_2SO_4) and 0.1 M sulfuric acid (H_2SO_4) was freshly prepared and sonicated for 30 min before use. The GOx was electrochemically reduced by cyclic voltammetry by scanning from 0.3V to -1.5 V for 15 cycles at a scan rate of 50 mVs^{-1}. A magnetic nickel (Ni) layer was deposited from a 1:1 (v/v) mixture of commercial platinum solution and nickel plating solution, containing 20 g L^{-1} $NiCl_2.6H_2O$, 515 g L^{-1} $Ni(H_2NSO_3)_2.4H_2O$, and 20 g L^{-1} H_3BO_3. The first Pt layer was deposited galvanostatically at –2 mA for 250 s from the commercial Pt plating solution, and for 200 s from the Pt-Ni solution. The intermediate Ni layer was deposited amperometrically at –1.3 V for 0.8 C from the Pt-Ni solution and for 1.6 C from the Ni plating solution. Finally, the inner Pt metallic layer was galvanostatically deposited from the Pt plating solution at –4 mA for 450 s. After carefully removing the gold layer by hand polishing with alumina slurry, the membrane was dissolved in methylene chloride to release the micromotors. The micromotors were finally washed with methylene chloride, ethanol and water, three times with each solvent. These will be referred to as the GOx/Ni/Pt microtubes.

The GOx/Ni/Pt/MnO_2 micromotors with an inner protective MnO_2 core were obtained by depositing MnO_2, after the deposition of the Pt layer. The deposition was carried out at +0.85 V for 180 s with a plating solution containing 100 mM manganese (II) acetate and 100 mM sodium sulfate in ultrapure water. The template removal and washing steps were performed as described earlier. To obtain SH/Au/GOx/Ni/Pt/MnO_2 micromotors, GOx/Ni/Pt/MnO_2 micromotors were sputter coated with a 10 nm gold layer. The Au-coated micromotors were functionalized using a 10 mM 1-octadecanethiol solution in ethanol and incubated at room temperature overnight. After the thiolation, the microtubes were washed thoroughly and stored for further studies.

4. RESULTS AND DISCUSSION

4.1. SYNTHESIS AND CHARACTERIZATION OF NOVEL MANGANESE OXIDE BASED MICROMOTORS [I, II]

Manganese oxide can be synthesized in different particle sizes, morphologies and geometrical shapes. The focus of this study was to prepare MnO_2 based well-defined geometries that could effectively undergo motion, such as microtubes, microrods and spherical particles. The synthesis of microtubes and microrods was performed by electrochemical deposition method, as illustrated in Figure 4A. The spherical MnO_2@$MnCO_3$ particles were prepared following the scheme shown in Figure 4B.

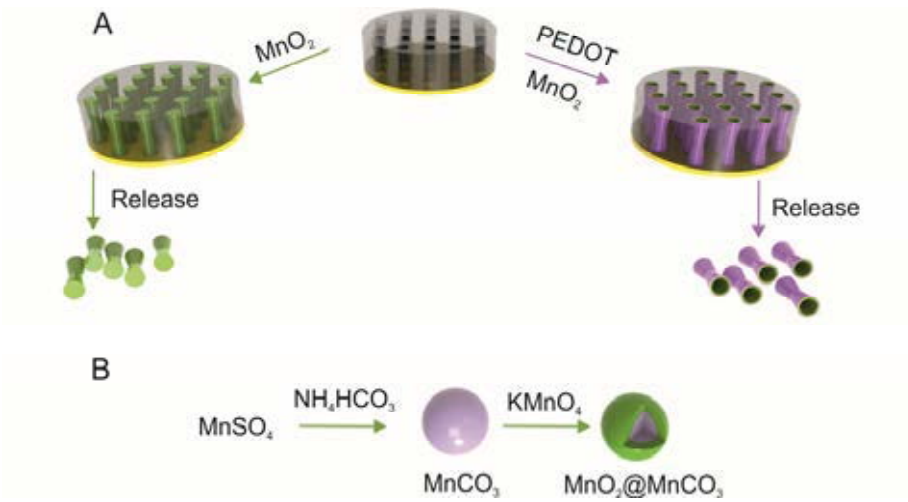

Figure 4. (A) Illustration of the preparation of MnO_2 microtubes and microrods by template-assisted electrodeposition method. (B) Synthesis of MnO_2@$MnCO_3$ spherical particles with co-precipitation.

The appearance and surface morphology of all types of prepared MnO_2 micromotors were analyzed by SEM. The $MnCO_3$ template particles had rather rough morphology, whereas, the MnO_2@$MnCO_3$ particles contained nanostructures on them. The removal of $MnCO_3$ core produced hollow MnO_2 particles. Synthesis of MnO_2 in tubular shape required an external layer of a conductive material (in this case PEDOT); otherwise, a rod-like geometry was obtained. Hydrothermal synthesis of MnO_2 produced porous particles with cross-linked nanosheets. The precursor $MnCO_3$ particles were converted into Mn_2O_3 by calcination. For comparison, commercially available MnO_2 particles were also included in the study. Figure 5 presents the SEM images of all the MnO_2 micromotors.

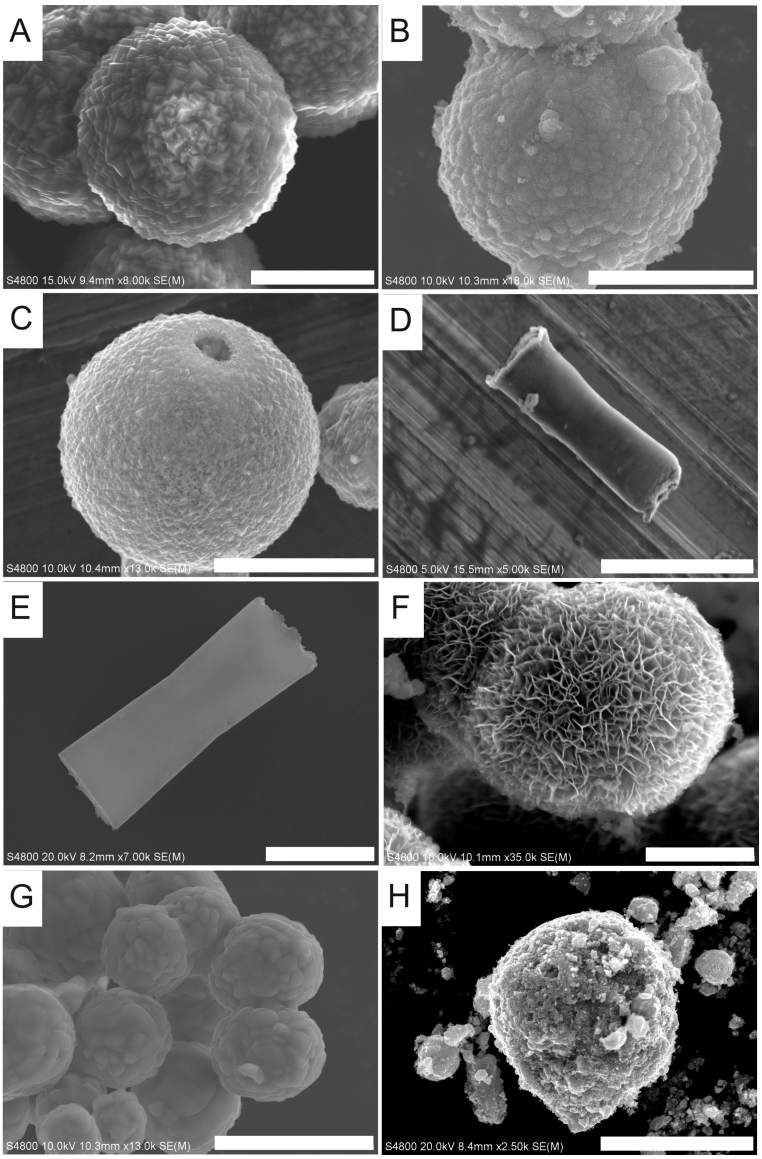

Figure 5. SEM images of MnO_2 micromotors. (A) $MnCO_3$ microsphere, (B) MnO_2@$MnCO_3$ microparticle, (C) hollow MnO_2 particle, (D) MnO_2 microtube, (E) MnO_2 microrod, (F) MnO_2 particle prepared by the hydrothermal method, (G) Mn_2O_3 particle after calcination of $MnCO_3$, (H) commercial MnO_2 microparticle. The scale bars are as follows; (A, E) 5 µm, (B) 3 µm, (C, G) 4 µm, (D) 10 µm, (F) 1 µm, and (H) 20 µm.

For the study of motion of the MnO_2 particles prepared, fuel concentrations of 1, 2, 5 and 10% were used, in the presence of 0.5% SDS or Triton X-100 as surfactant. In all cases, the speeds were averaged by tracking at least seven individual micromotors. In the presence of 1% fuel, MnO_2@$MnCO_3$ micromotors achieved the average speed of

~156 ± 38 μm s^{-1}. In 2% fuel, the micromotors exhibited a more rapid motion with relatively intense tails of bubbles. The average speed reached ~402 ± 175 μm s^{-1}. Upon further increasing the fuel concentration to 5 and 10%, the speeds reached ~468 μm s^{-1} and 586 μm s^{-1}, respectively, with the maximum recorded speed of the individual tracked micromotor motor being 987 μm s^{-1} at 10% H_2O_2. The particle size distribution as observed by SEM was 3-5 μm. Interestingly, single particles as well as particle aggregates (multimers) could move. The hollow MnO_2 particles obtained after the dissolution of $MnCO_3$ core from the MnO_2@$MnCO_3$ particles, were observed to undergo negligible motion at 1% and 2% fuel levels. However, in the presence of 5% H_2O_2, the average recorded speed was ~321 ± 58 μm s^{-1}. If the concentration of fuel was increased to 10%, the average recorded speed was ~996 ± 384 μm s^{-1}. The maximum speed of the individual hollow MnO_2 micromotor was 1625 μm s^{-1}. This is the highest speed observed for any catalytic MnO_2-based micromotor to date.

The electrochemically prepared microtubes and microrods could only move in the presence of at least 5% H_2O_2. The average speed of both types of micromotors was ~200 ± 80 μm s^{-1} (equal to ~16 body lengths s^{-1}). By increasing the fuel concentration up to 10%, the speeds increased to ~340 ± 73 μm s^{-1}. The MnO_2 particles prepared by hydrothermal method, with a particle size of 2-5 μm, could undergo random motion in the presence of at least 2% fuel, with a speed of ~339 ± 55 μm s^{-1}. At 5% and 10% fuel, the speeds were ~415 ± 107 μm s^{-1} and ~421 ± 132 μm s^{-1}, respectively. This trend represents that a speed plateau was reached and further increase in the fuel concentration did not cause any increase in the speed. The Mn_2O_3 particles also required at least 2% fuel to undergo a random motion. The observed average speeds for 2%, 5% and 10% H_2O_2 levels were ~308 ± 60 μm s^{-1}, ~328 ± 162 μm s^{-1} and ~474 ± 160 μm s^{-1}, respectively. The commercially available MnO_2 microparticles could move up to a speed of ~677 ± 239 μm s^{-1} in 10% fuel. A comparison of observed average speeds for all MnO_2 micromotors is presented in Figure 6.

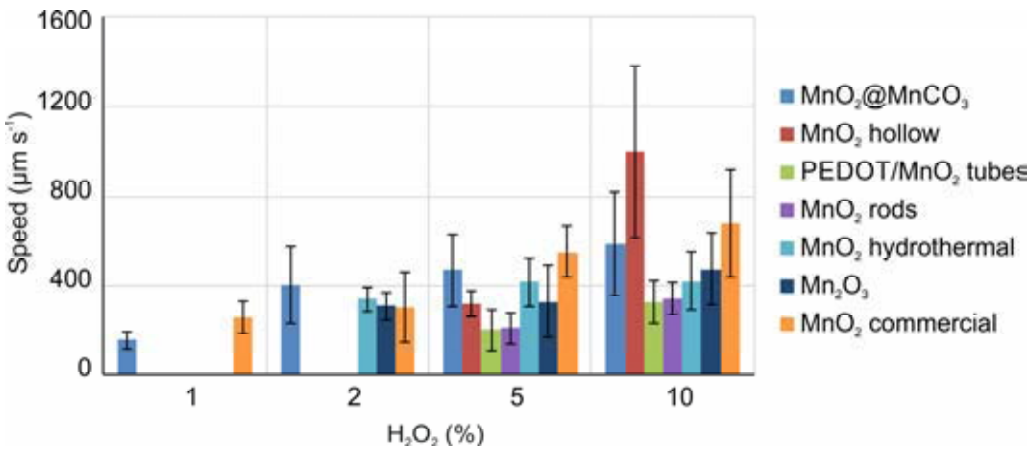

Figure 6. Average speeds of MnO_2 micromotors in different device architectures at different fuel concentrations (n = 7).

Except commercial MnO_2 particles, all the synthetic MnO_2 micromotors underwent self-degradation, with operational lifetime being dependent on the concentration of H_2O_2 used. The MnO_2@$MnCO_3$ motors could continue their motion even beyond 40 min, whereas, hollow MnO_2 particles decomposed in ~7 min, under a similar fuel level (*i.e.* 5%). The shorter lifetime in this case is expected to be due to the internal and external surfaces of the particles being in contact with the fuel, thereby increasing the rate of degradation. The lifetimes of the electrochemically prepared MnO_2 microtubes and microrods were up to 3 min and 13 min, respectively, which is merely dictated by the quantity of MnO_2 deposited. In the case of MnO_2 prepared by hydrothermal method, bubble formation disappeared in ~15 min. The propulsion of Mn_2O_3 particles continued for about 10 min in 5% fuel. The commercial MnO_2 particles continued to move as long as the fuel was present on the glass slide during the motion visualization experiment. Upon drying of the fuel droplet, a refueling led to reinitiating the motion by bubble formation. Their motion could last for up to 2 h. Figure 7 depicts the exemplary optical images of the motion of MnO_2 microtubes, microrods and spherical MnO_2@$MnCO_3$ particles.

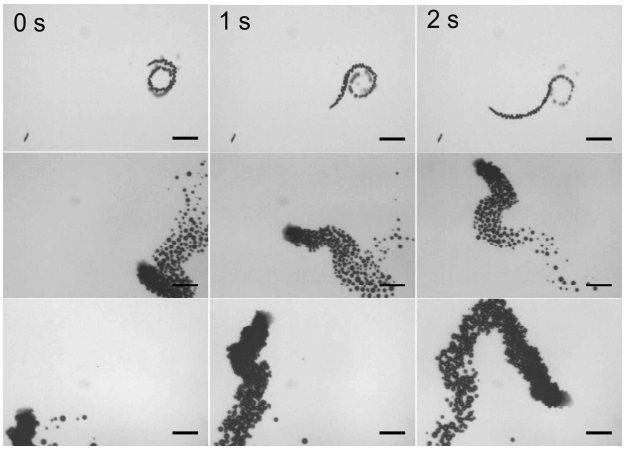

Figure 7. Time-lapse optical images of moving microtubes (top), microrods (middle) and MnO_2@$MnCO_3$ particles (bottom) in 5% H_2O_2 and 0.5% surfactant.

There can be several reasons behind the differences in the speeds among the different types of MnO_2 micromotors, such as the influence of the particle size and shape as well as the surface morphology. However, the differences are more likely attributed to the presence of different crystalline forms of MnO_2 (polymorphism). Polymorphism can lead to different catalytic activities among different types of MnO_2 micromotors and hence vary the decomposition rates of H_2O_2 fuel. To investigate the type of polymorphs in each case, the MnO_2 particles were subjected to XRD analysis.

The diffraction pattern of the MnO_2@$MnCO_3$ particles produced very intense peaks due to the highly crystalline $MnCO_3$ core, which completely suppressed the peaks belonging to MnO_2. The hollow MnO_2 microparticles, prepared by dissolving the $MnCO_3$ core of

the MnO_2@$MnCO_3$ particles, were determined to be ε-MnO_2 with a low degree of crystallinity, as also reported in the literature.[110] Thus, the core-shell MnO_2@$MnCO_3$ particles and hollow MnO_2 particles were composed of the same ε-MnO_2. Surprisingly, hollow MnO_2 particles required rather higher concentration of the fuel to undergo motion, compared to MnO_2@$MnCO_3$ particles. At low fuel concentrations, bubble forming hollow MnO_2 microparticles remained floating without noticeable random motion. In 10% fuel, their random motion was the fastest amongst all types of MnO_2 particles. The MnO_2 synthesized by electrochemical method was found to be very amorphous in nature and did not produce any diffraction pattern (data not shown), as also noticed in other studies.[111] Such type of MnO_2 was found to be the least efficient, requiring at least 5% H_2O_2 for efficient motion. At lower concentrations, the bubble formation was observed but did not result in any motion. The hydrothermal MnO_2 was characterized as birnessite-type (δ-MnO_2) and contained K, Mn and O, as confirmed by EDX elemental mapping. The Mn_2O_3 particles were of high crystallinity and their propulsion efficiency was similar to birnessite-type (δ-MnO_2), but less than the ε-MnO_2. The commercially obtained MnO_2 was also identified to be ε-MnO_2. It must be noted that it was only the ε-MnO_2 among all the tested polymorphs, which led to the effective propulsion even at 1% of H_2O_2. The reason for the prolonged lifetime of the commercial particles is not yet understood. Figure 8 shows the XRD patterns of different MnO_2 polymorphs prepared in this study.

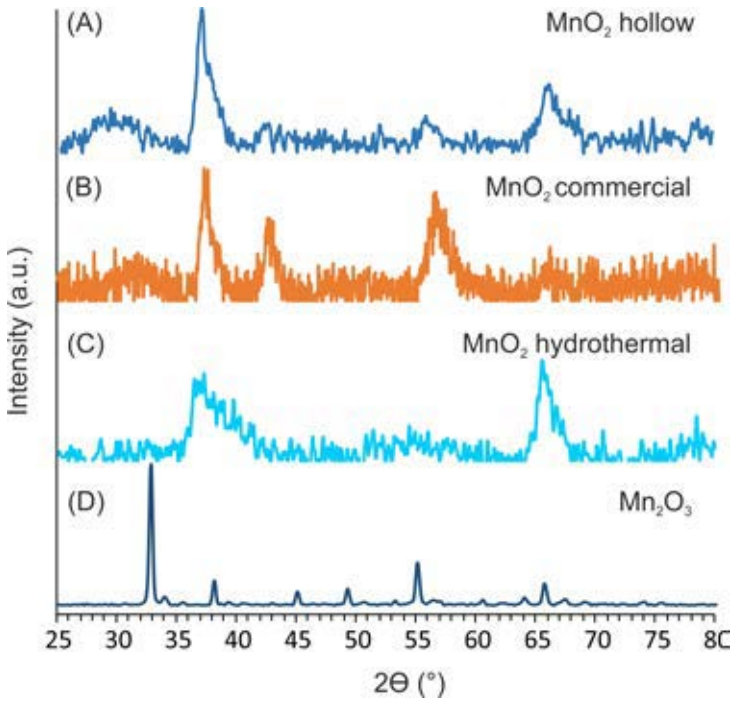

Figure 8. XRD analysis of synthetic and commercial MnO_2 particles.

The chemical reaction of MnO_2 with H_2O_2 is very complex and can be either catalytic or non-catalytic in nature, based on the solution pH.[112] A neutral of alkaline pH favors a catalytic reaction, but an acidic pH causes a non-catalytic reaction to occur, which results in the degradation of MnO_2 particles. An acidic pH of the H_2O_2 solution might be responsible for the occurrence of a non-catalytic reaction. Some general reactions of MnO_2 and H_2O_2 are given as follows,[113] which explain the decomposition of MnO_2 particles.

$$MnO_2 + H_2O_2 + 2H^+ \rightarrow Mn^{2+} + 2H_2O + O_2 \uparrow$$

$$Mn^{2+} + 2H_2O_2 \leftrightarrows Mn(OH)_2 + 2H^+$$

$$Mn(OH)_2 + H_2O_2 \rightarrow MnO_2 + 2H_2O$$

Besides the polymorphic form of the MnO_2 particles, the size and geometrical design also influences the propulsion. Wang *et. al*. recently studied the effect of microtubular dimensions on propulsion.[114] However, no such studies yet exist about bubble- propelled spherical micromotors. The micromotors essentially require an asymmetry to undergo motion. The tubular micromotors with an outer PEDOT layer are chemically asymmetric because only the inner part of the motors is catalytically active. The bubble formation and ejection leads to a net displacement of the microtube. On the other hand, microrods and spherical MnO_2 particles are chemically symmetric, but the presence of geometrical defects and inhomogeneity result in a certain level of geometrical asymmetry, which favors bubble formation/nucleation at some parts compared to the remaining parts of the motor. Interestingly, electrochemically prepared microtubes and microrods differ with regards to the device designs but their speeds were comparable. This may be because they both were composed of the amorphous MnO_2. This indicates that the crystalline form plays a decisive role in determining the propulsion efficiency. The ε-MnO_2 micromotors could also efficiently move in an environment that contained 37 mg/mL of NaCl or 7 mg/mL of bovine serum albumin. Both of these additives are known to fully deactivate Pt based micromotors.[115,116]

4.2. REMOVAL OF ORGANIC DYES FROM POLLUTED WATER [III]

The shape and surface morphology of the commercially obtained MnO_2 particles were examined by using SEM. The particles were polydispersed and structurally asymmetric with a rough morphology. The ability of these particles to act as micromotors was then investigated by adding SDS containing solution of H_2O_2. Upon the addition of fuel, the particles started to intensely produce bubbles and underwent a random motion for extended periods of time (Figure 9). In 5% H_2O_2, the average speed of the micromotors (n = 7) was ~551 ± 115 μm s^{-1} (*i.e.*, ~55 body lengths s^{-1}), with a maximum recorded speed of ~720 μm s^{-1}.

Figure 9. Time-lapse optical images of the autonomous propulsion of MnO_2 micromotors in 5% H_2O_2 and 0.1% SDS.

The water remediation by MnO_2 can be based on two distinct mechanisms. The decomposition of H_2O_2 by MnO_2 micromotors produces radicals that can remove organic pollutants by chemical degradation (CD).[117] In parallel, the dye molecules may adsorb onto the O_2 bubbles and a dye-rich foam is produced through a phenomena known as adsorptive bubble separation (ABS), as illustrated in Figure 10. The experiments were performed using 5% H_2O_2 and 0.1% SDS as the initial test condition. Methylene blue (MB) and Rhodamine 6G were selected as model organic pollutants because these are widely used in the textile industry and the waste water is excessively discharged into the environment.[118,119] To study CD of MB and R6G, MnO_2 particles were incubated with aqueous solutions of the dyes and H_2O_2, without adding SDS. Immediately upon fuel addition, a rapid generation of bubbles started which continued for over several minutes, then gradually slowed down and eventually stopped. The reaction vessel was left un-agitated for 1 h, followed by collecting an aliquot of the solution for visible light absorption spectroscopy analysis. The effect of the fuel concentration on CD of MB was also studied by varying the concentration of H_2O_2. The data suggests that the concentration of oxidant had negligible effect on CD of MB.

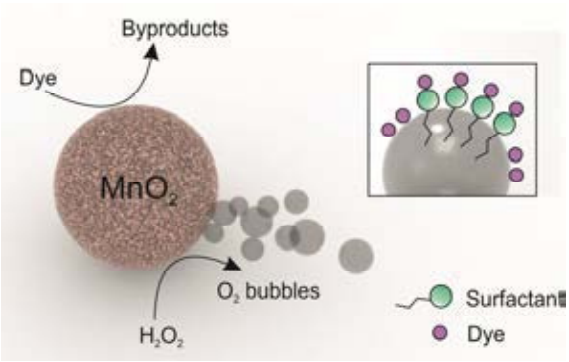

Figure 10. Graphical depiction of the removal of organic dyes by MnO_2 micromotors through catalytic CD and ABS processes. The inset shows adsorption of dye molecules at the bubble–air interface.

To study an additional ABS of the dyes (*i.e.*, a dual effect by combining CD and ABS), an aqueous solution of SDS was added to the samples before the addition of H_2O_2. The quantities of the reagents were adjusted to obtain 5% fuel and 0.1% SDS in a 10 mL of

total reaction volume. In the presence of surfactant, the bubble generation led to the formation of thick foam of several inches at the top of the dye solution. The color of the foam gradually turned darker as the dye adsorption progressed. After 1 h, an aliquot was taken out of the reaction solution for absorption spectroscopy. The dye solution became nearly colorless after a combined CD/ABS experiment, whereas after CD only, a noticeable amount of the intact dye molecules remained present in solution. The absorption spectroscopy profiles and physical appearance of the dye solutions before and after CD and CD/ABS are shown in Figure 11.

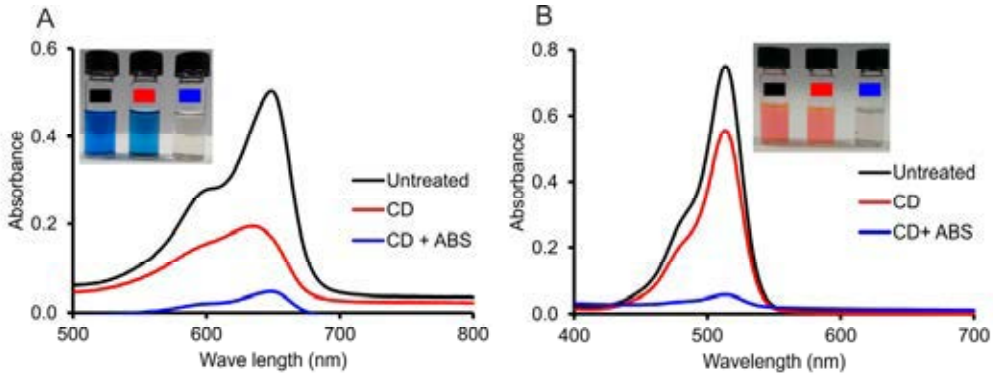

Figure 11. Visible light absorption profiles of (A) methylene blue and (B) Rhodamine 6G dyes before and after catalytic degradation (CD) and adsorptive bubble separation (ABS). Inset shows the appearance of the corresponding solutions.

The MnO_2 micromotors caused 29% and 66% decolorization of R6G and MB, respectively, by CD in 1 h of reaction time. However, a combined CD/ABS led to above 90% decolorization for both dyes. In the absence of SDS, the bubble formation disappeared in ca. 30 min, observed visually. However, in the presence of surfactant, bubble formation was facilitated over an hour. Once all the fuel is consumed, addition of fresh H_2O_2 reinitiates the bubble formation.

To examine the actual mechanism of CD with MB, the reaction mixtures before and after the decolorization experiment were analyzed by electrospray ionization mass spectrometry (ESI-MS). The mass spectra confirmed the partial degradation of the dye molecules, mainly through losses of methyl groups, which is consistent with the Fenton-like degradation of MB, reported previously.[120] On the other hand, ABS follows physical adsorption of dye molecules onto gas bubbles.[117,121] SDS being an anionic surfactant can electrostatically interact with positively charged dye molecules. As a result, the dye molecules may adsorb on the bubble surface at the gas–liquid interface, and are separated from the aqueous solution to the accumulated foam. The efficiency of decolorization remained consistent even if a mixture of both dyes was used.

4.3. PROTECTION OF PLATINUM BASED MICROMOTORS FROM THIOL TOXICITY [IV]

Here, we demonstrate the use of manganese oxide (MnO_2) as a protective layer on the Pt surface to avoid thiol-induced catalyst deactivation. Microtubes based on the outer graphene oxide (GOx) and the inner Pt layers were synthesized, followed by MnO_2 deposition to completely block the pores at the final stage of the fabrication process. Upon dissolution of the polycarbonate template, the released micromotors were washed, dried and sputtered with a thin Au layer to allow functionalization of the surface with 1-octadecanethiol. Finally, the protective MnO_2 layer was removed by H_2O_2 treatment resulting in bare tubular Au-functionalized Pt micromotors. The micromotors protected with MnO_2 could move with high speeds, while the unprotected micromotors were completely deactivated under the same conditions. Figure 12 illustrates the operation of the protected micromotors with MnO_2.

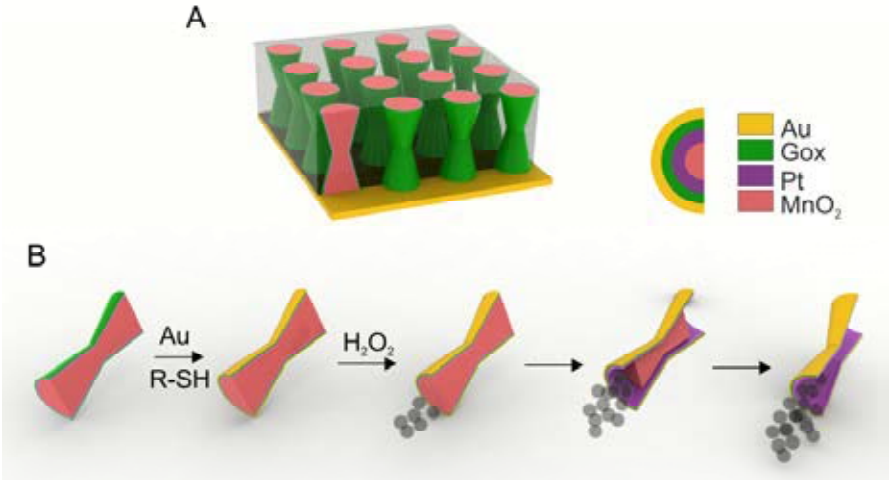

Figure 12. Schematic of the protected micromotors with a MnO_2 core.

Both GOx/Ni/Pt and GOx/Ni/Pt/MnO_2 micromotors were characterized with SEM-EDS to visualize their morphology and to observe the distribution of MnO_2 inside the microtubes (Figure 13). Upon the addition of H_2O_2 fuel to the GOx/Ni/Pt/MnO_2 micromotors, the MnO_2 started to decompose H_2O_2 and the formation of bubbles was readily noticed. As a result, the micromotors started to move. The reaction of MnO_2 with H_2O_2 also causes a degradation of the MnO_2 structure, resulting in the opening of the tubular cavity and exposing the Pt surface to the fuel. The micromotors containing the protective MnO_2 core are initially slow because MnO_2 mediates the bubble formation, which occurs at the rear end of the microtube, but as soon as the MnO_2 core starts to degrade, the micromotor speed gradually increases. In our case, the speeds reached the peak levels in ca. 10 minutes when MnO_2 was completely depleted, and the Pt layer started to catalyze the bubble formation. Therefore, the determination of particle speeds was conducted at least 20 min after the fuel addition to ensure complete removal

of MnO_2. The GOx/Ni/Pt control micromotors without the MnO_2 core rapidly started to move with high speeds because the Pt layer was fully active from the very beginning of the experiment.

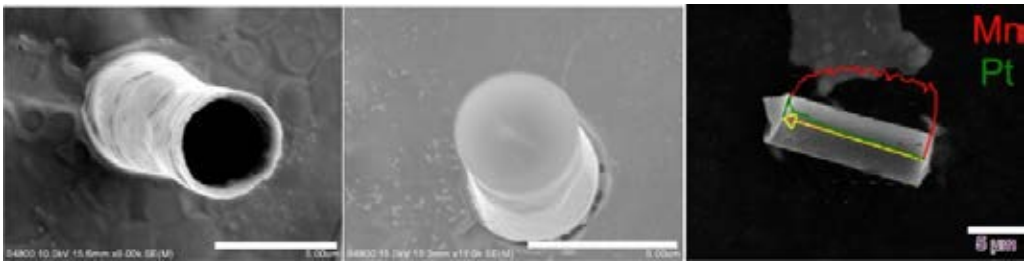

Figure 13. SEM images of the GOx/Ni/Pt (left) and GOx/Ni/Pt/MnO_2 (middle) microtubes. The EDS scan lines of Mn and Pt are shown for the latter particles (right). Scale bars are 5 µm.

A comparison of the average speeds (n = 10) of the micromotors with and without the protective MnO_2 core is presented in Figure 14. The average speeds of the micromotors with the MnO_2 core (after 20 min of operation) were very similar to the control micromotors (no MnO_2 deposited) in a range of fuel concentrations tested.

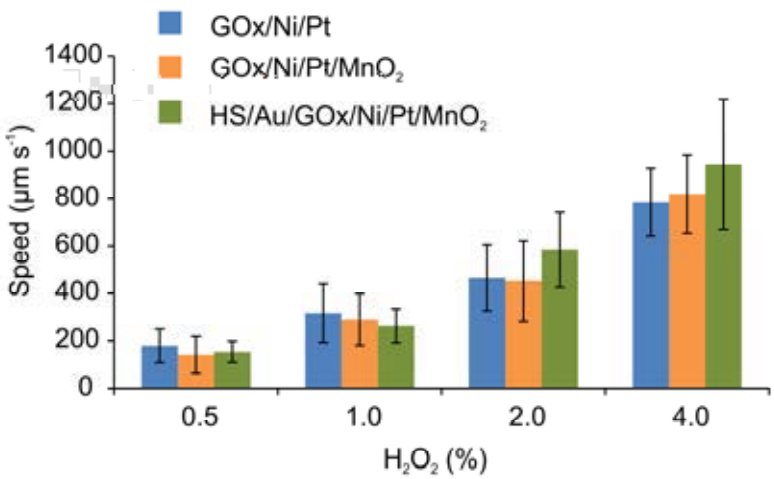

Figure 14. Average speeds of GOx/Ni/Pt microtubes in different fuel concentrations and 0.1% SDS: without MnO_2 core (blue) as control, with MnO_2 core (orange) and with MnO_2 core after functionalization with 1-octadecanethiol (green).

In order to test the effectiveness of the approach to protect Pt from thiol toxicity, the micromotors were coated with a thin Au film. After the overnight incubation of the microtubes in 1-octadecanethiol, the visualization of motion was conducted. As expected, no motion could be noticed by the GOx/Ni/Pt micromotors due to the

complete deactivation of the Pt surface with 1-dodecanethiol molecules. Even when a fuel concentration was raised to 30%, the micromotors seldom moved, although some bubble formation was in fact observed. On the contrary, the GOx/Ni/Pt/MnO_2 micromotors underwent a highly consistent motion, without any compromise of their speeds (as compared to the control microtubes) in all fuel concentrations tested.

To demonstrate an application of the prepared microtubes, an oil/water emulsion was prepared by gently mixing high-grade vacuum pump oil in ultrapure water (1:20, v/v) with 0.1% sodium dodecyl sulphate (SDS) serving as surfactant. An aliquot of 1 µl of the microtubes were pipetted onto a cleaned glass slide, followed by the addition of H_2O_2 and SDS solutions with final concentrations of 2% and 0.1%, respectively. Then, 1 µl of oil/water emulsion was added. The capture and transport of the oil droplets were performed to demonstrate a cargo transport capability of the thiol-functionalized Au/GOx/Ni/Pt micromotors (Figure 15).

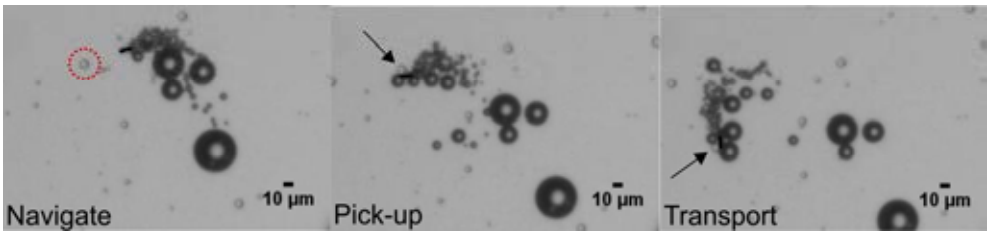

Figure 15. Navigation, pick-up and transport of an oil droplet by the HS/Au/GOx/Ni/Pt/MnO_2 micromotor.

5. CONCLUSIONS

A majority of catalytic MNMs are typically based on extremely rare elements, such as Pt. Despite of its excellent catalytic activity, Pt experiences some serious limitations, such as a drastically reduced motion in salt rich environments and in the presence of proteins. Moreover, Pt is a very expensive material, which limits its widespread use in practical applications. Therefore, new materials for MNMs are constantly sought.

MnO_2 is a very low-cost and abundant material that decomposes H_2O_2 to produce O_2 gas, similar to Pt. Therefore, MnO_2 holds a significant potential to be used for the preparation of novel micromotors. In this study, a variety of MnO_2-based micromotors were synthesized and characterized. Their motion was studied in different chemical environments. Most of the micromotors prepared could undergo motion in the presence of at least 2% H_2O_2 fuel. Both MnO_2@$MnCO_3$ and commercial MnO_2 microparticles, composed of ε-MnO_2, could move even at 1% of H_2O_2. However, the hollow MnO_2 particles, which were also ε-MnO_2, underwent clear random motion only at >5% H_2O_2. In 10% fuel, these were the fastest moving micromotors among all. The reason behind this behavior is not known. The electrochemically prepared MnO_2 microtubes and microrods were amorphous and exhibited a poor propulsion behavior. Though, a tubular geometry favors a bubble propulsion by facilitating the bubble growth, the speeds of MnO_2 microtubes and microrods were similar. Thus, the polymorphic form of MnO_2 plays a decisive role in governing the propulsion characteristics. Hence, the choice of the fabrication method and synthesis parameters deserve a careful attention when preparing MnO_2-based micromotors. The ε-MnO_2 micromotors can efficiently move also in salt rich environment or in the presence of proteins, which highlights another benefit of this material.

We demonstrated a novel application of MnO_2 micromotors for the removal of organic dyes from contaminated water. The application was based on catalytic degradation of the dye molecules without or with adsorptive bubble formation. A combined dual effect of MnO_2 micromotors, that is, CD/ABS, resulted in marked decolorization of the contaminated water samples. Above 90% decolorization was reached in just 1 h, which was followed by an almost complete decolorization in an extended period of time without a need of an external agitation. The study holds a great promise for MnO_2 microparticle-based water remediation at the industrial scale and even in remote field locations where mechanical mixing is not feasible.

We also presented a proof-of-concept solution for the protection of Pt-based micromotors against thiol-induced deactivation, which limits their functionalization by gold–thiol chemistry for a variety of applications. The inner catalytic surface of the electrochemically fabricated Au/Pt micromotors was covered with a core of MnO_2 to completely block the pore opening. This approach protects the inner Pt surface from the chemisorption of thiols. The outer Au surface was functionalized with an alkanethiol, followed by the simple removal of the protective MnO_2 layer by a simple

H_2O_2 treatment. The unprotected micromotors were completely deactivated due to the thiol chemisorption on the Pt surface. On the other hand, the motion of the protected micromotors remained unaffected after the incubation with an alkanethiol. Thus, the use of MnO_2 represents a simple and effective means for the protection of Pt surface against the thiol toxicity and should find widespread use for the preparation of functional Pt-based tubular micromotors for various applications.

The research presented in this thesis highlights a great potential of MnO_2 for the preparation of micromotors. However, different polymorphs of MnO_2 exhibit varying catalytic efficiency to lead to a propulsion. Thus, it is noteworthy to pay a careful attention to the choice of a synthesis method and reaction parameters for obtaining a polymorph that would result in an efficient motion. The MnO_2 particles can be used for the removal of non-biodegradable organic dyes from contaminated water. Such a low-cost, non-toxic and abundant material that can also be commercially obtained in bulk quantities, holds a great advantage over the other materials for MNMs-based practical applications. In addition, MnO_2 can be used for the protection of electrochemically prepared Pt based micromotors against the thiol-induced toxicity.

Future studies can be directed to further improve the propulsion efficiency and/or operational lifetime of different MnO_2 polymorphs. Also, diverse applications of MnO_2-based micromotors need to be explored, such as transient microscale mixers to enhance diffusion-limited processes, removal of toxic heavy metals, etc.

Despite all the features of micromotors and their potential for various applications, there are some limitations as well. A complete recovery of non-degradable micromotors from the environment after the accomplishment of a remediation task will be crucial to avoid any secondary contamination. In case the micromotors could be separated by using an external magnetic field, appropriate equipment should be designed that could be applicable also to remote field location. If the micromotors are transient and self-decomposable, their products should be environment friendly. Also, the currently demonstrated environmental applications of micromotors are still at the proof-of-concept level. Thus, scaled-up applications need to be demonstrated.

ACKNOWLEDGEMENTS

This research work was conducted during 2014–2017 at the Department of Chemistry, University of Eastern Finland. The financial support from the Faculty of Science and Forestry of the University of Eastern Finland is gratefully acknowledged.

I am very grateful to my supervisor Prof. Janne Jänis for his utmost support at all stages. It has been a very productive experience to work as his team member. I am also grateful to Prof. Tapani Pakkanen, Prof. Mika Suvanto and Prof. Juha Rouvinen for their trust and support. I thank the entire staff at the Department of Chemistry, particularly Dr. Sari Suvanto, Ms. Päivi Inkinen, Ms. Tarja Virantalo and Ms. Mari Heiskanen for their help and guidance. I also offer my deepest gratitude to Prof. Jaakko Timonen and Prof. Hélder A. Santos for critically reading this thesis and their suggested improvements.

I would like to acknowledge Prof. Wei Gao from California Institute of Technology, Prof. Samuel Sanchez from Institute for Bioengineering of Catalonia, and Dr. Lluís Soler from Universitat Politècnica de Catalunya, for their help and support. I am also grateful to Prof. Jesse Greener from Laval University, Quebec, and Dr. Juliane Simmchen from Technical University of Dresden, for a fruitful collaboration. I thank my teammates Dr. Niko Kinnunen, Dr. Mikko Laitaoja, Mr. Owies Mukhtar Wani, Mr. Tam Do Minh and Mr. Shahid Ullah Khan for their interest in my research and a dedicated work. It was a team work that enabled a contribution to the field. I also thank Dr. Tommi Itkonen from the Department of Physics, for his support.

I dedicate my thesis to my late parents Mr. Ilam-ud-din and Ms. Shahnaz Akhtar, and to all my teachers who educated and inspired me, particularly Prof. Najam-ul-Haq from Bahauddin Zakariya University, Multan – Pakistan. I extend my respect and regards to my family, particularly to my elder brothers who supported me during the times of hardship. I present my love and affection to my wife Hafiza Sajida Kousar and my daughter Rameen Safdar for their continuous support and care. I am also highly grateful to all my friends and colleagues who are always a great source of encouragement for me.

Joensuu, November 2017. *Muhammad Safdar*

REFERENCES

1. David, S. *Fantastic Voyage*; Twentieth Century Fox Film Corporation, 1966.

2. Sengupta, S.; Ibele, M. E.; Sen, A. Fantastic Voyage: Designing Self-Powered Nanorobots. *Angew. Chem. Int. Ed.* **2012**, *51* (34), 8434–8445.

3. Schliwa, M.; Woehlke, G. Molecular Motors. *Nature* **2003**, *422* (6933), 759–765.

4. Chattopadhyay, S.; Moldovan, R.; Yeung, C.; Wu, X. L. Swimming Efficiency of Bacterium Escherichia Coli. *Proc. Natl. Acad. Sci.* **2006**, *103* (37), 13712–13717.

5. Guix, M.; Mayorga-martinez, C. C.; Merkoc, A. Nano/Micromotors in (Bio) Chemical Science Applications. *Chem. Rev.* **2014**, *114* (12), 6285–6322.

6. Feynman, R. P. There's Plenty of Room at the Bottom. *Eng. Sci.* **1960**, *23*, 22–36.

7. Ozin, G. A.; Manners, I.; Fournier-Bidoz, S.; Arsenault, A. Dream Nanomachines. *Adv. Mater.* **2005**, *17* (24), 3011–3018.

8. Baylis, J. R.; Yeon, J. H.; Thomson, M. H.; Kazerooni, A.; Wang, X.; St. John, A. E.; Lim, E. B.; Chien, D.; Lee, A.; Zhang, J. Q.; et al. Self-Propelled Particles That Transport Cargo through Flowing Blood and Halt Hemorrhage. *Sci. Adv.* **2015**, *1* (9), e1500379.

9. Delezuk, J. A. M.; Ramírez-Herrera, D. E.; Esteban-Fernández de Ávila, B.; Wang, J. Chitosan-Based Water-Propelled Micromotors with Strong Antibacterial Activity. *Nanoscale* **2017**, *9* (6), 2195–2200.

10. Li, J.; Angsantikul, P.; Liu, W.; Esteban-Fernandez de Avila, B.; Thamphiwatana, S.; Xu, M.; Sandraz, E.; Wang, X.; Delezuk, J.; Gao, W.; et al. Micromotors Spontaneously Neutralize Gastric Acid for pH-Responsive Payload Release. *Angew. Chem. Int. Ed.* **2017**, *56* (8), 2156–2161.

11. Li, J.; Singh, V. V; Sattayasamitsathit, S.; Orozco, J.; Kaufmann, K.; Dong, R.; Gao, W.; Jurado-sanchez, B.; Fedorak, Y.; Wang, J. Water-Driven Micromotors for Rapid Photocatalytic Degradation of Biological and Chemical Warfare Agents. *ACS Nano* **2014**, *8* (11), 11118–11125.

12. Qiu, T.; Lee, T.-C.; Mark, A. G.; Morozov, K. I.; Münster, R.; Mierka, O.; Turek, S.; Leshansky, A. M.; Fischer, P. Swimming by Reciprocal Motion at Low Reynolds Number. *Nat. Commun.* **2014**, *5*, 5119.

13. Purcell, E. M. Life at Low Reynolds Number. *Am. J. Phys.* **1977**, *45*, 3–11.

14. Fusco, S.; Ullrich, F.; Pokki, J.; Chatzipirpiridis, G.; Ozkale, B.; Sivaraman, K. M.; Ergeneman, O.; Pané, S.; Nelson, B. J. Microrobots: A New Era in Ocular Drug Delivery. *Expert Opin. Drug Deliv.* **2014**, *11* (11), 1815–1826.

15. Nelson, B. J., Ioannis, K. K., Jake, J. A. Microrobots for Minimally Invasive Medicine. *Annu. Rev. Biomed. Eng.* **2010**, *12* (1), 55–85.

16. Qiu, F.; Nelson, B. J. Magnetic Helical Micro- and Nanorobots: Toward Their Biomedical Applications. *Engineering* **2015**, *1* (1), 21–26.

17. Bell, D. J.; Leutenegger, S.; Hammar, K. M.; Dong, L. X.; Nelson, B. J. Flagella-like Propulsion for Microrobots Using a Nanocoil and a Rotating Electromagnetic Field. *Proc. IEEE Int. Conf. Robot. Autom.* **2007**, *April*, 1128–1133.

18. Mushtaq, F.; Guerrero, M.; Sakar, M. S.; Hoop, M.; Lindo, A. M.; Sort, J.; Chen, X.; Nelson, B. J.; Pellicer, E.; Pané, S. Magnetically Driven Bi_2O_3/BiOCl-Based Hybrid Microrobots for Photocatalytic Water Remediation. *J. Mater. Chem. A* **2015**, *3* (47), 23670–23676.

19. Tottori, S.; Zhang, L.; Qiu, F.; Krawczyk, K. K.; Franco-Obregõn, A.; Nelson, B. J. Magnetic Helical Micromachines: Fabrication, Controlled Swimming, and Cargo Transport. *Adv. Mater.* **2012**, *24* (6), 811–816.

20. Safdar, M.; Simmchen, J.; Jänis, J. Light-Driven Micro- and Nanomotors for Environmental Remediation. *Environ. Sci. Nano* **2017**, *4*, 1602–1616.

21. Liu, M.; Zentgraf, T.; Liu, Y.; Bartal, G.; Zhang, X. Light-Driven Nanoscale Plasmonic Motors. *Nat. Nanotechnol.* **2010**, *5* (8), 570–573.

22. Búzás, A.; Kelemen, L.; Mathesz, A.; Oroszi, L.; Vizsnyiczai, G.; Vicsek, T.; Ormos, P. Light Sailboats: Laser Driven Autonomous Microrobots. *Appl. Phys. Lett.* **2012**, *101*, 41111.

23. Abid, J.; Frigoli, M.; Pansu, R.; Szeftel, J.; Zyss, J.; Larpent, C.; Brasselet, S. Light-Driven Directed Motion of Azobenzene-Coated Polymer Nanoparticles in an Aqueous Medium. *Langmuir* **2011**, *27*, 7967–7971.

24. Yang, P. P.; Zhai, Y. G.; Qi, G. Bin; Lin, Y. X.; Luo, Q.; Yang, Y.; Xu, A. P.; Yang, C.; Li, Y. S.; Wang, L.; et al. NIR Light Propulsive Janus-like Nanohybrids for Enhanced Photothermal Tumor Therapy. *Small* **2016**, *12* (39), 5423–5430.

25. He, W.; Frueh, J.; Hu, N.; Liu, L.; Gai, M.; He, Q. Guidable Thermophoretic Janus Micromotors Containing Gold Nanocolorifiers for Infrared Laser Assisted Tissue Welding. *Adv. Sci.* **2016**, *3* (12), 1600206.

26. Ibele, M.; Mallouk, T. E.; Sen, A. Schooling Behavior of Light-Powered Autonomous Micromotors in Water. *Angew. Chem. Int. Ed.* **2009**, *48* (18), 3308–3312.

27. Hong, Y.; Diaz, M.; Córdova-Fteueroa, U. M.; Sen, A. Light-Driven Titanium-Dioxide-Based Reversible Microfireworks and Micromotor/micropump Systems. *Adv. Funct. Mater.* **2010**, *20* (10), 1568–1576.

28. Jang, B.; Hong, A.; Kang, H. E.; Alcantara, C.; Charreyron, S.; Mushtaq, F.; Pellicer, E.; Büchel, R.; Sort, J.; Lee, S. S.; et al. Multiwavelength Light-Responsive Au/B-TiO_2 Janus Micromotors. *ACS Nano* **2017**, *11* (6), 6146–6154.

29. Huang, H.-W.; Sakar, M. S.; Petruska, A. J.; Pané, S.; Nelson, B. J. Soft Micromachines with Programmable Motility and Morphology. *Nat. Commun.* **2016**, *7*, 12263.

30. Uchida, E.; Azumi, R.; Norikane, Y. Light-Induced Crawling of Crystals on a Glass Surface. *Nat. Commun.* **2015**, *6*, 7310.

31. Ding, X.; Lin, S.-C. S.; Kiraly, B.; Yue, H.; Li, S.; Chiang, I.-K.; Shi, J.; Benkovic, S. J.; Huang, T. J. On-Chip Manipulation of Single Microparticles, Cells, and Organisms Using Surface Acoustic Waves. *Proc. Natl. Acad. Sci.* **2012**, *109* (28), 11105–11109.

32. Rao, K. J.; Li, F.; Meng, L.; Zheng, H.; Cai, F.; Wang, W. A Force to Be Reckoned With: A Review of Synthetic Microswimmers Powered by Ultrasound. *Small* **2015**, *11* (24), 2836–2846.

33. Wang, W.; Castro, L. A.; Hoyos, M.; Mallouk, T. E. Autonomous Motion of Metallic Microrods Propelled by Ultrasound. *ACS Nano* **2012**, *6* (7), 6122–6132.

34. Garcia-Gradilla, V.; Orozco, J.; Sattayasamitsathit, S.; Soto, F.; Kuralay, F.; Pourazary, A.; Katzenberg, A.; Gao, W.; Shen, Y. F.; Wang, J. Functionalized Ultrasound-Propelled Magnetically Guided Nanomotors: Toward Practical Biomedical Applications. *ACS Nano* **2013**, *7* (10), 9232–9240.

35. Ahmed, S.; Gentekos, D. T.; Fink, C. A.; Mallouk, T. E. Self-Assembly of Nanorod Motors into Geometrically Regular Multimers and Their Propulsion by Ultrasound. *ACS Nano* **2014**, *8* (11), 11053–11060.

36. Wang, W.; Duan, W.; Ahmed, S.; Mallouk, T. E.; Sen, A. Small Power: Autonomous Nano- and Micromotors Propelled by Self-Generated Gradients. *Nano Today* **2013**, *8* (5), 531–534.

37. Moran, J. L.; Posner, J. D. Phoretic Self-Propulsion. *Annu. Rev. Fluid Mech.* **2017**, *49* (1), 511–540.

38. Jang, B.; Wang, W.; Wiget, S.; Petruska, A. J.; Chen, X.; Hu, C.; Hong, A.; Folio, D.; Ferreira, A.; Pané, S.; et al. Catalytic Locomotion of Core-Shell Nanowire Motors. *ACS Nano* **2016**, *10* (11), 9983–9991.

39. Ma, X.; Katuri, J.; Zeng, Y.; Zhao, Y.; Sanchez, S. Surface Conductive Graphene-Wrapped Micromotors Exhibiting Enhanced Motion. *Small* **2015**, *11*, 5023–2027.

40. Hong, Y.; Velegol, D.; Chaturvedi, N.; Sen, A. Biomimetic Behavior of Synthetic Particles: From Microscopic Randomness to Macroscopic Control. *Phys. Chem. Chem. Phys.* **2010**, *12*, 1423–1435.

41. Duan, W.; Liu, R.; Sen, A. Transition between Collective Behaviors of Micromotors in Response to Different Stimuli. *J. Am. Chem. Soc.* **2013**, *135* (4), 1280–1283.

42. Paxton, W. F.; Sen, A.; Mallouk, T. E. Motility of Catalytic Nanoparticles through Self-Generated Forces. *Chem. Eur. J.* **2005**, *11* (22), 6462–6470.

43. Lee, T. C.; Alarcón-Correa, M.; Miksch, C.; Hahn, K.; Gibbs, J. G.; Fischer, P. Self-Propelling Nanomotors in the Presence of Strong Brownian Forces. *Nano Lett.* **2014**, *14* (5), 2407–2412.

44. Solovev, A. A.; Mei, Y. F.; Urena, E. B.; Huang, G. S.; Schmidt, O. G. Catalytic Microtubular Jet Engines Self-Propelled by Accumulated Gas Bubbles. *Small* **2009**, *5* (14), 1688–1692.

45. Solovev, A. A.; Smith, E. J.; Bufon, C. C. B.; Sanchez, S.; Schmidt, O. G. Light-Controlled Propulsion of Catalytic Microengines. *Angew. Chem. Int. Ed.* **2011**, *50* (46), 10875–10878.

46. Gao, W.; Sattayasamitsathit, S.; Orozco, J.; Wang, J. Highly Efficient Catalytic Microengines: Template Electrosynthesis of Polyaniline/Platinum Microtubes. *J. Am. Chem. Soc.* **2011**, *133* (31), 11862–11864.

47. Wang, H.; Zhao, G. J.; Pumera, M. Crucial Role of Surfactants in Bubble-Propelled Microengines. *J. Phys. Chem. C* **2014**, *118* (10), 5268–5274.

48. Ismagilov, R. F.; Schwartz, A.; Bowden, N.; Whitesides, G. M. Autonomous Movement and Self-Assembly. *Angew. Chem. Int. Ed.* **2002**, *41* (4), 652–654.

49. Laocharoensuk, R.; Burdick, J.; Wang, J. Carbon-Nanotube-Induced Acceleration of Catalytic Nanomotors. *ACS Nano* **2008**, *2* (5), 1069–1075.

50. Howse, J. R.; Jones, R. A. L.; Ryan, A. J.; Gough, T.; Vafabakhsh, R.; Golestanian, R. Self-Motile Colloidal Particles: From Directed Propulsion to Random Walk. *Phys. Rev. Lett.* **2007**, *99* (4), 48102.

51. Choudhury, U.; Soler, L.; Gibbs, J. G.; Sanchez, S.; Fischer, P. Surface Roughness-Induced Speed Increase for Active Janus Micromotors. *Chem. Commun.* **2015**, *51*, 8660–8663.

52. Sanchez, S.; Ananth, A. N.; Fomin, V. M.; Viehrig, M.; Schmidt, O. G. Superfast Motion of Catalytic Microjet Engines at Physiological Temperature. *J. Am. Chem. Soc.* **2011**, *133* (38), 14860–14863.

53. Tu, Y.; Peng, F.; White, P. B.; Wilson, D. A. Redox-Sensitive Stomatocyte Nanomotors: Destruction and Drug Release in the Presence of Glutathione. *Angew. Chem. Int. Ed.* **2017**, *56* (26), 7620–7624.

54. Tu, Y.; Peng, F.; Sui, X.; Men, Y.; White, P. B.; van Hest, J. C. M.; Wilson, D. A. Self-

Propelled Supramolecular Nanomotors with Temperature-Responsive Speed Regulation. *Nat. Chem.* **2016**, *9* (5), 480–486.

55. Tu, Y.; Peng, F.; André, A. A. M.; Men, Y.; Srinivas, M.; Wilson, D. A. Biodegradable Hybrid Stomatocyte Nanomotors for Drug Delivery. *ACS Nano* **2017**, *11* (2), 1957–1963.

56. Guix, M.; Orozco, J.; Garcia, M.; Gao, W.; Sattayasamitsathit, S.; Merkoči, A.; Escarpa, A.; Wang, J. Superhydrophobic Alkanethiol-Coated Microsubmarines for Effective Removal of Oil. *ACS Nano* **2012**, *6* (5), 4445–4451.

57. Liu, M.; Liu, L.; Gao, W.; Su, M.; Ge, Y.; Shi, L.; Zhang, H.; Dong, B.; Li, C. Y. A Micromotor Based on Polymer Single Crystals and Nanoparticles: Toward Functional Versatility. *Nanoscale* **2014**, *6* (15), 8601–8605.

58. Wang, H.; Zhao, G.; Pumera, M. Beyond Platinum: Bubble-Propelled Micromotors Based on Ag and MnO_2 Catalysts. *J. Am. Chem. Soc.* **2014**, *136* (7), 2719–2722.

59. Gao, W.; Uygun, A.; Wang, J. Hydrogen-Bubble-Propelled Zinc-Based Microrockets in Strongly Acidic Media. *J. Am. Chem. Soc.* **2012**, *134* (2), 897–900.

60. Sattayasamitsathit, S.; Kou, H.; Gao, W.; Thavarajah, W.; Kaufmann, K.; Zhang, L.; Wang, J. Fully Loaded Micromotors for Combinatorial Delivery and Autonomous Release of Cargoes. *Small* **2014**, *10* (14), 2830–2833.

61. Mou, F.; Chen, C.; Ma, H.; Yin, Y.; Wu, Q.; Guan, J. Self-Propelled Micromotors Driven by the Magnesium-Water Reaction and Their Hemolytic Propertiem. *Angew. Chem. Int. Ed.* **2013**, *52* (28), 7208–7212.

62. Gao, W.; Feng, X.; Pei, A.; Gu, Y.; Li, J.; Wang, J. Seawater-Driven Magnesium Based Janus Micromotors for Environmental Remediation. *Nanoscale* **2013**, *5* (11), 4696–4700.

63. Gao, W.; Pei, A.; Wang, J. Water-Driven Micromotors. *ACS Nano* **2012**, *6* (9), 8432–8438.

64. Feng, X.; Zhang, Y.; Li, Y.; Huang, Z.; Chen, S.; Ma, Y.; Zhang, L.; Wang, L.; Yan, X. Graphene-Based Highly Efficient Micromotors. *Chem. Lett.* **2015**, *44* (3), 399–401.

65. Chen, X.; Wu, G.; Lan, T.; Chen, W. Autonomous Micromotors Based on Catalytically Pneumatic Behavior of Balloon-like MnO_x–graphene crumples. *Chem. Commun.* **2014**, *50*, 7157–7159.

66. Mou, F.; Pan, D.; Chen, C.; Gao, Y.; Xu, L.; Guan, J. Magnetically Modulated Pot-Like MnFe2O4 Micromotors: Nanoparticle Assembly Fabrication and Their Capability for Direct Oil Removal. *Adv. Funct. Mater.* **2015**, *25* (39), 6173–6181.

67. Singh, A. K.; Mandal, T. K.; Bandyopadhyay, D. Magnetically Guided Chemical

Locomotion of Self-Propelling Paperbots. *RSC Adv.* **2015**, *5* (79), 64444–64449.

68. Sanchez, S.; Solovev, A. A.; Mei, Y.; Schmidt, O. G. Dynamics of Biocatalytic Microengines Mediated by Variable Friction Control. *J. Am. Chem. Soc.* **2010**, *132* (38), 13144–13145.

69. Gu, Y.; Sattayasamitsathit, S.; Kaufmann, K.; Vazquez-Duhalt, R.; Gao, W.; Wang, C.; Wang, J. Self-Propelled Chemically-Powered Plant-Tissue Biomotors. *Chem. Commun.* **2013**, *49* (66), 7307.

70. Ma, X.; Jannasch, A.; Albrecht, U. R.; Hahn, K.; Miguel-Lopez, A.; Schaffer, E.; Sanchez, S. Enzyme-Powered Hollow Mesoporous Janus Nanomotors. *Nano Lett.* **2015**, *15* (10), 7043–7050.

71. Ma, X.; Wang, X.; Hahn, K.; Sánchez, S. Motion Control of Urea-Powered Biocompatible Hollow Microcapsules. *ACS Nano* **2016**, *10* (3), 3597–3605.

72. Ma, X.; Hortelao, A. C.; Miguel-Lopez, A.; Sanchez, S. Bubble-Free Propulsion of Ultrasmall Tubular Nanojets Powered by Biocatalytic Reactions. *J. Am. Chem. Soc.* **2016**, *138* (42), 13782–13785.

73. Soler, L.; Martinez-Cisneros, C.; Swiersy, A.; Sanchez, S.; Schmidt, O. G. Thermal Activation of Catalytic Microjets in Blood Samples Using Microfluidic Chips. *Lab Chip* **2013**, *13* (22), 4299–4303.

74. Song, Y.; Liu, Z.; Kong, T.; Shum, H. C. Micromotors with Built-in Compasses. *Chem. Commun.* **2013**, *49* (17), 1726–1728.

75. Ahmed, S.; Wang, W.; Mair, L. O.; Fraleigh, R. D.; Li, S.; Castro, L. A.; Hoyos, M.; Huang, T. J.; Mallouk, T. E. Steering Acoustically Propelled Nanowire Motors toward Cells in a Biologically Compatible Environment Using Magnetic Fields. *Langmuir* **2013**, *29* (52), 16113–16118.

76. Zhao, G.; Pumera, M. Geometric Asymmetry Driven Janus Micromotors. *Nanoscale* **2014**, *6* (19), 11177–11180.

77. Safdar, M.; Itkonen, T.; Janis, J. Bubble-Propelled Trimetallic Microcaps as Functional Catalytic Micromotors. *RSC Adv.* **2015**, *5* (17), 13171–13174.

78. Zhao, G.; Ambrosi, A.; Pumera, M. Self-Propelled Nanojets via Template Electrodeposition. *Nanoscale* **2013**, *5*, 1319–1324.

79. Gao, W.; Sattayasamitsathit, S.; Uygun, A.; Pei, A.; Ponedal, A.; Wang, J. Polymer-Based Tubular Microbots: Role of Composition and Preparation. *Nanoscale* **2012**, *4* (7), 2447.

80. Paxton, W. F.; Kistler, K. C.; Olmeda, C. C.; Sen, A.; St Angelo, S. K.; Cao, Y. Y.; Mallouk, T. E.; Lammert, P. E.; Crespi, V. H. Catalytic Nanomotors: Autonomous

Movement of Striped Nanorods. *J. Am. Chem. Soc.* **2004**, *126* (41), 13424–13431.

81. Tu, Y.; Peng, F.; André, A. A. M.; Men, Y.; Srinivas, M.; Wilson, D. A. Biodegradable Hybrid Stomatocyte Nanomotors for Drug Delivery. *ACS Nano* **2017**, *11* (2), 1957–1963.

82. Fei, J.; Cui, Y.; Yan, X.; Qi, W.; Yang, Y.; Wang, K.; He, Q.; Li, J. Controlled Preparation of MnO_2 Hierarchical Hollow Nanostructures and Their Application in Water Treatment. *Adv. Mater.* **2008**, *20* (3), 452–456.

83. del Mercato, L. L.; Carraro, M.; Zizzari, A.; Bianco, M.; Miglietta, R.; Arima, V.; Viola, I.; Nobile, C.; Sorarù, A.; Vilona, D.; et al. Catalytic Self-Propulsion of Supramolecular Capsules Powered by Polyoxometalate Cargos. *Chem. Eur. J.* **2014**, *20* (35), 10910–10914.

84. Wu, Y.; Lin, X.; Wu, Z.; Möhwald, H.; He, Q. Self-Propelled Polymer Multilayer Janus Capsules for Effective Drug Delivery and Light-Triggered Release. *ACS Appl. Mater. Interfaces* **2014**, *6* (13), 10476–10481.

85. Peng, F.; Tu, Y.; Van Hest, J. C. M.; Wilson, D. A. Self-Guided Supramolecular Cargo-Loaded Nanomotors with Chemotactic Behavior towards Cells. *Angew. Chem. Int. Ed.* **2015**, *54* (40), 11662–11665.

86. Li, J.; Esteban-Fernández de Ávila, B.; Gao, W.; Zhang, L.; Wang, J. Micro/nanorobots for Biomedicine: Delivery, Surgery, Sensing, and Detoxification. *Sci. Robot.* **2017**, *2* (4), eaam6431.

87. Xuan, M.; Shao, J.; Lin, X.; Dai, L.; He, Q. Self-Propelled Janus Mesoporous Silica Nanomotors with Sub-100 nm Diameters for Drug Encapsulation and Delivery. *ChemPhysChem* **2014**, *15* (11), 2255–2260.

88. Wu, Z.; Wu, Y.; He, W.; Lin, X.; Sun, J.; He, Q. Self-Propelled Polymer-Based Multilayer Nanorockets for Transportation and Drug Release. *Angew. Chem. Int. Ed.* **2013**, *52* (27), 7000–7003.

89. Mou, F. Z.; Chen, C. R.; Zhong, Q.; Yin, Y. X.; Ma, H. R.; Guan, J. G. Autonomous Motion and Temperature-Controlled Drug Delivery of Mg/Pt-Poly(N-Isopropylacrylamide) Janus Micromotors Driven by Simulated Body Fluid and Blood Plasma. *ACS Appl. Mater. Interfaces* **2014**, *6* (12), 9897–9903.

90. Gao, W.; Dong, R.; Thamphiwatana, S.; Li, J.; Gao, W.; Zhang, L.; Wang, J. Artificial Micromotors in the Mouse's Stomach: A Step toward in Vivo Use of Synthetic Motors. *ACS Nano* **2014**, *9* (1), 117–123.

91. de Ávila, B. E.-F.; Angsantikul, P.; Li, J.; Angel Lopez-Ramirez, M.; Ramírez-Herrera, D. E.; Thamphiwatana, S.; Chen, C.; Delezuk, J.; Samakapiruk, R.; Ramez, V.; et al. Micromotor-Enabled Active Drug Delivery for in Vivo Treatment of Stomach Infection. *Nat. Commun.* **2017**, *8* (1), 272.

92. Li, J.; Thamphiwatana, S.; Liu, W.; Esteban-Fernandez De Avila, B.; Angsantikul, P.; Sandraz, E.; Wang, J.; Xu, T.; Soto, F.; Ramez, V.; et al. Enteric Micromotor Can Selectively Position and Spontaneously Propel in the Gastrointestinal Tract. *ACS Nano* **2016**, *10* (10), 9536–9542.

93. Sanchez, S.; Solovev, A. a; Schulze, S.; Schmidt, O. G. Controlled Manipulation of Multiple Cells Using Catalytic Microbots. *Chem. Commun.* **2011**, *47* (2), 698–700.

94. Campuzano, S.; Orozco, J.; Kagan, D.; Guix, M.; Gao, W.; Sattayasamitsathit, S.; Claussen, J. C.; Merkoçi, A.; Wang, J. Bacterial Isolation by Lectin-Modified Microengines. *Nano Lett.* **2012**, *12* (1), 396–401.

95. Orozco, J.; Cortes, A.; Cheng, G. Z.; Sattayasamitsathit, S.; Gao, W.; Feng, X. M.; Shen, Y. F.; Wang, J. Molecularly Imprinted Polymer-Based Catalytic Micromotors for Selective Protein Transport. *J. Am. Chem. Soc.* **2013**, *135* (14), 5336–5339.

96. García, M.; Orozco, J.; Guix, M.; Gao, W.; Sattayasamitsathit, S.; Escarpa, A.; Merkoçi, A.; Wang, J. Micromotor-Based Lab-on-Chip Immunoassays. *Nanoscale* **2013**, *5*, 1325–1331.

97. Yu, X.; Li, Y.; Wu, J.; Ju, H. Motor-Based Autonomous Microsensor for Motion and Counting Immunoassay of Cancer Biomarker. *Anal. Chem.* **2014**, *86* (9), 4501–4507.

98. Morales-Narváez, E.; Guix, M.; Medina-Sánchez, M.; Mayorga-Martinez, C. C.; Merkoçi, A. Micromotor Enhanced Microarray Technology for Protein Detection. *Small* **2014**, *10* (13), 2542–2548.

99. Vilela, D.; Orozco, J.; Cheng, G.; Sattayasamitsathit, S.; Galarnyk, M.; Kan, C.; Wang, J.; Escarpa, A. Multiplexed Immunoassay Based on Micromotors and Microscale Tags. *Lab Chip* **2014**, *14* (18), 3505.

100. Solovev, A. a.; Xi, W.; Gracias, D. H.; Harazim, S. M.; Deneke, C.; Sanchez, S.; Schmidt, O. G. Self-Propelled Nanotools. *ACS Nano* **2012**, *6* (2), 1751–1756.

101. Soler, L.; Magdanz, V.; Fomin, V. M.; Sanchez, S.; Schmidt, O. G. Self-Propelled Micromotors for Cleaning Polluted Water. *ACS Nano* **2013**, *7* (11), 9611–9620.

102. Orozco, J.; Cheng, G.; Vilela, D.; Sattayasamitsathit, S.; Vazquez-Duhalt, R.; Valdés-Ramírez, G.; Pak, O. S.; Escarpa, A.; Kan, C.; Wang, J. Micromotor-Based High-Yielding Fast Oxidative Detoxification of Chemical Threats. *Angew. Chem. Int. Ed.* **2013**, *52* (50), 13276–13279.

103. Singh, V. V; Kaufmann, K.; Orozco, J.; Li, J.; Galarnyk, M.; Arya, G.; Wang, J. Micromotor-Based on-off Fluorescence Detection of Sarin and Soman Simulants. *Chem. Commun.* **2015**, *51* (56), 11190–11193.

104. Vilela, D.; Parmar, J.; Zeng, Y.; Zhao, Y.; Sanchez, S. Graphene Based Microbots for Toxic Heavy Metal Removal and Recovery from Water. *Nano Lett.* **2016**, *16* (4), 2860–

2866.

105. Uygun, D. A.; Jurado-Sánchez, B.; Uygun, M.; Wang, J. Self-Propelled Chelation Platforms for Efficient Removal of Toxic Metals. *Environ. Sci. Nano* **2016**, *3* (3), 559–566.

106. Ge, Y.; Liu, M.; Liu, L.; Sun, Y.; Zhang, H.; Dong, B. Dual-Fuel-Driven Bactericidal Micromotor. *Nano-Micro Lett.* **2016**, *8* (2), 157–164.

107. Orozco, J.; Pan, G.; Sattayasamitsathit, S.; Galarnyk, M.; Wang, J. Micromotors to Capture and Destroy Anthrax Simulant Spores. *Analyst* **2015**, *140* (5), 1421–1427.

108. Schindelin, J.; Arganda-Carreras, I.; Frise, E.; Kaynig, V.; Longair, M.; Pietzsch, T.; Preibisch, S.; Rueden, C.; Saalfeld, S.; Schmid, B.; et al. Fiji: An Open-Source Platform for Biological-Image Analysis. *Nat. Meth.* **2012**, *9* (7), 676–682.

109. Chen, R.; Yu, J.; Xiao, W. Hierarchically Porous MnO_2 Microspheres with Enhanced Adsorption Performance. *J. Mater. Chem. A* **2013**, *1* (38), 11682–11690.

110. Han, D.; Jing, X.; Xu, P.; Ding, Y.; Liu, J. Facile Synthesis of Hierarchical Hollow ε-MnO_2 Spheres and Their Application in Supercapacitor Electrodes. *J. Solid State Chem.* **2014**, *218*, 178–183.

111. Liu, R.; Sang, B. L. MnO_2/poly(3,4-Ethylenedioxythiophene) Coaxial Nanowires by One-Step Coelectrodeposition for Electrochemical Energy Storage. *J. Am. Chem. Soc.* **2008**, *130* (10), 2942–2943.

112. Do, S. H.; Batchelor, B.; Lee, H. K.; Kong, S. H. Hydrogen Peroxide Decomposition on Manganese Oxide (Pyrolusite): Kinetics, Intermediates, and Mechanism. *Chemosphere* **2009**, *75* (1), 8–12.

113. Broughton, B. D.; Wentworth, R. L. Mechanism of Decomposition of Hydrogen Peroxide Solutions with Manganese Dioxide. *J. Am. Chem. Soc.* **1947**, *69*, 741–744.

114. Wang, H.; Moo, J. G. S.; Pumera, M. From Nanomotors to Micromotors: The Influence of the Size of an Autonomous Bubble-Propelled Device upon Its Motion. *ACS Nano* **2016**, *10* (5), 5041–5050.

115. Wang, H.; Zhao, G.; Pumera, M. Blood Proteins Strongly Reduce the Mobility of Artificial Self-Propelled Micromotors. *Chem. Eur. J.* **2013**, *19* (49), 16756–16759.

116. Zhao, G. J.; Wang, H.; Khezri, B.; Webster, R. D.; Pumera, M. Influence of Real-World Environments on the Motion of Catalytic Bubble-Propelled Micromotors. *Lab Chip* **2013**, *13* (15), 2937–2941.

117. Zhang, L.; Nie, Y.; Hu, C.; Hu, X. Decolorization of Methylene Blue in Layered Manganese Oxide Suspension with H_2O_2. *J. Hazard. Mater.* **2011**, *190* (1–3), 780–785.

118. Demir, N.; Gönduz, G.; Dukkanci, M. Degradation of a Textile Dye, Rhodamine 6G (Rh6G), by Heterogeneous sonophotoFenton Process in the Presence of Fe-Containing TiO_2 Catalysts. *Environ. Sci .Pollut. Res.* **2015**, *22* (5), 3193–3201.

119. Muthuraman, G.; Teng, T. T.; Leh, C. P.; Norli, I. Extraction and Recovery of Methylene Blue from Industrial Wastewater Using Benzoic Acid as an Extractant. *J. Hazard. Mater.* **2009**, *163* (1), 363–369.

120. Zhao, G.; Li, J.; Ren, X.; Hu, J.; Hu, W.; Wang, X. Highly Active MnO_2 Nanosheet Synthesis from Graphene Oxide Templates and Their Application in Efficient Oxidative Degradation of Methylene Blue. *RSC Adv.* **2013**, *3* (31), 12909.

121. Horng, J.; Huang, S. Removal of Organic Dye (Direct Blue) from Synthetic Wastewater by Adsorptive Bubble Separation Techniques. *Environ. Sci. Technol.* **1993**, *27* (6), 1169–1175.

112/2012 KORHONEN Tuulia: The wettability properties of nano- and micromodified paint surfaces
113/2012 JOKI-KORPELA Fatima: Functional polyurethane-based films and coatings
114/2012 LAURILA Elina: Non-covalent interactions in Rh, Ru, Os, and Ag complexes
115/2012 MAKSIMAINEN Mirko: Structural studies of *Trichoderma reesei*, *Aspergillus oryzae* and *Bacillus circulans* sp. *alkalophilus* beta-galactosidases – Novel insights into a structure-function relationship
116/2012 PÖLLÄNEN Maija: Morphological, thermal, mechanical, and tribological studies of polyethylene composites reinforced with micro– and nanofillers
117/2013 LAINE Anniina: Elementary reactions in metallocene/methylaluminoxane catalyzed polyolefin synthesis
118/2013 TIMONEN Juri: Synthesis, characterization and anti-inflammatory effects of substituted coumarin derivatives
119/2013 TAKKUNEN Laura: Three-dimensional roughness analysis for multiscale textured surfaces: Quantitative characterization and simulation of micro- and nanoscale structures
120/2014 STENBERG Henna: Studies of self-organizing layered coatings
121/2014 KEKÄLÄINEN Timo: Characterization of petroleum and bio-oil samples by ultrahigh-resolution Fourier transform ion cyclotron resonance mass spectrometry
122/2014 BAZHENOV Andrey: Towards deeper atomic-level understanding of the structure of magnesium dichloride and its performance as a support in the Ziegler-Natta catalytic system
123/2014 PIRINEN Sami: Studies on $MgCl_2$/ether supports in Ziegler–Natta catalysts for ethylene polymerization
124/2014 KORPELA Tarmo: Friction and wear of micro-structured polymer surfaces
125/2014 HUOVINEN Eero: Fabrication of hierarchically structured polymer surfaces
126/2014 EROLA Markus: Synthesis of colloidal gold and polymer particles and use of the particles in preparation of hierarchical structures with self-assembly
127/2015 KOSKINEN Laura: Structural and computational studies on the coordinative nature of halogen bonding
128/2015 TUIKKA Matti: Crystal engineering studies of barium bisphosphonates, iodine bridged ruthenium complexes, and copper chlorides
129/2015 JIANG Yu: Modification and applications of micro-structured polymer surfaces
130/2015 TABERMAN Helena: Structure and function of carbohydrate-modifying enzymes
131/2015 KUKLIN Mikhail S.: Towards optimization of metalocene olefin polymerization catalysts via structural modifications: a computational approach
132/2015 SALSTELA Janne: Influence of surface structuring on physical and mechanical properties of polymer-cellulose fiber composites and metal-polymer composite joints
133/2015 CHAUDRI Adil Maqsood: Tribological behavior of the polymers used in drug delivery devices
134/2015 HILLI Yulia: The structure-activity relationship of Pd-Ni three-way catalysts for H_2S suppression
135/2016 SUN Linlin: The effects of structural and environmental factors on the swelling behavior of Montmorillonite-Beidellite smectics: a molecular dynamics approach
136/2016 OFORI Albert: Inter- and intramolecular interactions in the stabilization and coordination of palladium and silver complexes: DFT and QTAIM studies
137/2016 LAVIKAINEN Lasse: The structure and surfaces of 2:1 phyllosilicate clay minerals
138/2016 MYLLER Antti T.: The effect of a coupling agent on the formation of area-selective monolayers of iron α-octabutoxy phthalocyanine on a nano-patterned titanium dioxide carrier
139/2016 KIRVESLAHTI Anna: Polymer wettability properties: their modification and influences upon water movement
140/2016 LAITAOJA Mikko: Structure-function studies of zinc proteins
141/2017 NISSINEN Ville: The roles of multidentate ether and amine electron donors in the crystal structure formation of magnesium chloride supports